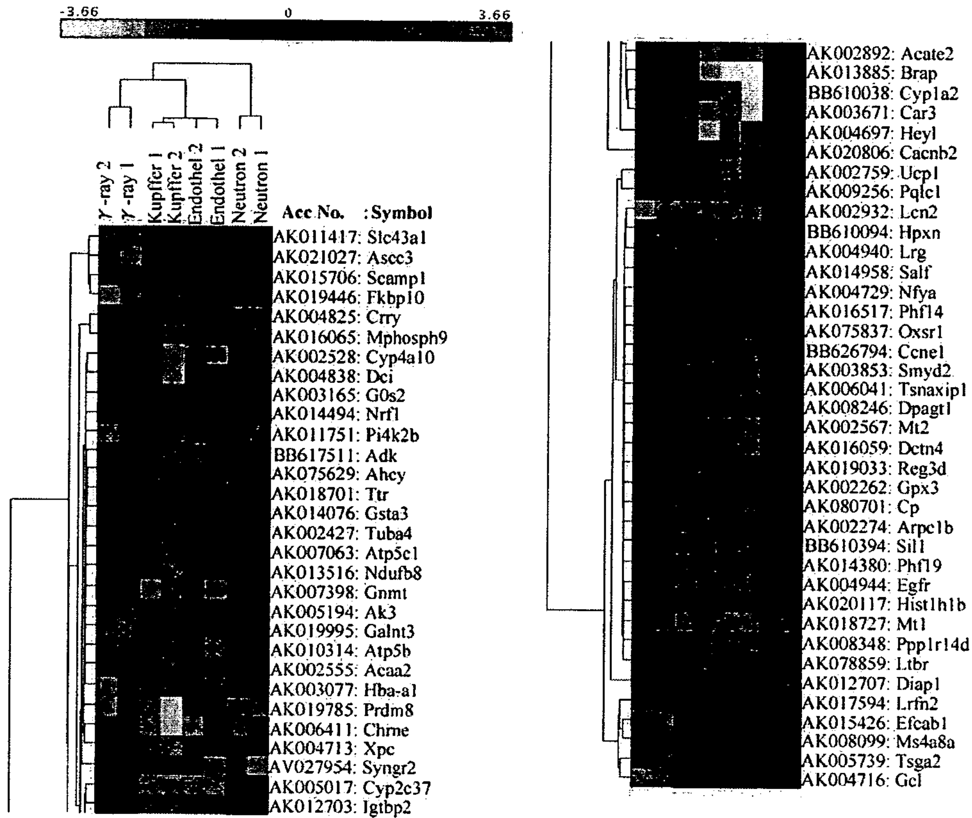

Fig. 2. Cluster analysis of individual mice according to the profile of gene expression examined. Mice from the same exposure group was the closest and the neutron exposure group was the most different from other groups.

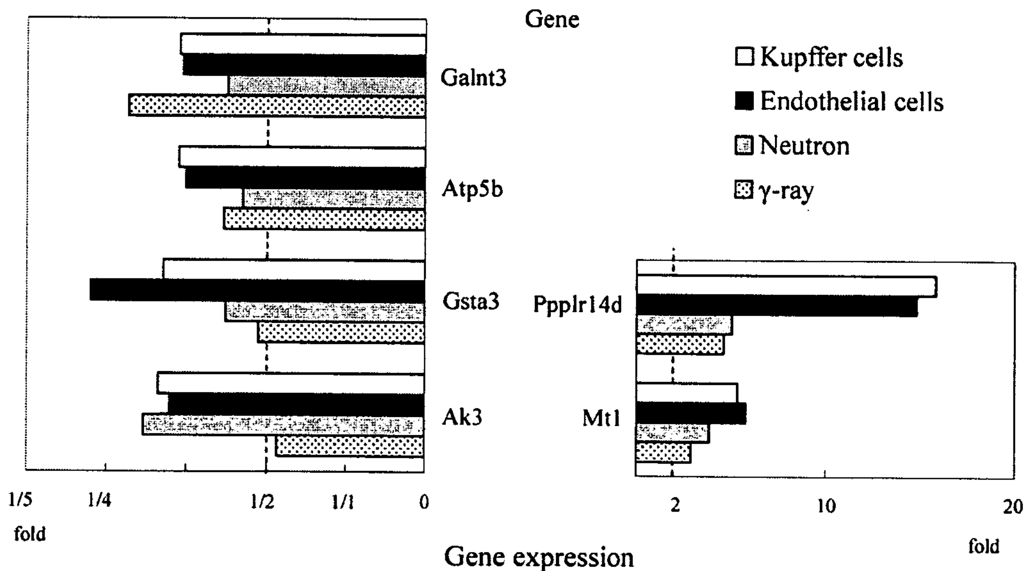

Fig. 3. Genes which are commonly over-expressed more than 2-fold or under-expressed less than a half following irradiation compared to control gene expression levels. Ak3: Adenylate kinase 3α, Gsta3: Glutathione S-transferase 3α, Atp5b: ATP synthase β subunit, Galnt3: UDP-N-acetyl-α-D-galactosamine-polypeptide, Mt1: Metallothionein 1, Ppp1r14d: Protein phosphatase 1, regulatory (inhibitor) subunit 14D.

(261), apoptosis (260), cardiovascular disease (240), neuroscience (197), toxicology/pharmacology (184), extracellular matrix/adhesion molecules (105), diabetes/obesity (105), developmental/regenerative disorder (102), cell cycle (99), and others (2,503).

After total RNA was extracted from the liver using TRIZOL reagent (Invitrogen Corp., Carlsbad, CA), Poly-A RNA was separated using dT(25)-coupled magnetic beads (Dynal Biotech, Oslo, Norway). Individual mice were evaluated for the change in gene expression against pooled liver RNA

Table 2-A. Up and down-regulated genes in all the irradiated groups

	Gene	Symbol	GenBank	Function
Up	Metallothionein 1	Mt1	AK018727	Metal binding
	Protein phosphatase 1, regulatory (inhibitor) subunit 14D	Ppp1r14d	AK008348	Protein phosphatase inhibitor
Down	Adenylate kinase 3α	Ak3	AK005194	Adenine metaboilsm
	Glutathione S-transferase α3	Gsta3	AK014076	Detoxication
	ATP synthase β subunit	Atp5b	AK010314	ATP synthesis
	UDP-N-acetyl-α-D-galactosamine-polypeptide	Galnt3	AK019995	Secretion

Table 2-B. Commonly up and down-regulated genes by Kupffer cell specific and endothelial cell specific exposures to α-particles

	Gene	Symbol	GenBank	Function
Up	Lipocalin 2	Lcn2	AK002932	Anti-apoptosis
	Metallothionein 2	Mt2	AK002567	Metal binding
	Actin related protein 2/3 complex, subunit 1B	Arpc1b	AK002274	Cytoskeleton, protein trafficking
	Dynactin 4	Dctn4	AK016059	Cytoskeleton, protein trafficking
	PHD finger protein 19	Phf19	AK014380	Chromatin regulation
	Epidermal growth factor receptor	Egfr	AK004944	Cell growth
	SET and MYND domain containing 2	Smyd2	AK003853	Transcription
	Endoplasmic reticulum chaperone SIL1 homolog	Sil1-pening	BB610394	Molecular chaperon
	Hemopexin	Hpxn	BB610094	Metal transporter, antioxidant
	Ceruloplasmin	Cp	AK080701	Metal transporter
	Cyclin E1	Ccne1	BB626794	Cell cycle
	Translin-associated factor X (Tsnax) interacting protein 1	Tsnaxip1	AK006041	Cell cycle
	Regenerating islet-derived δ	Reg3d	AK019033	Cell growth
	Glutathione peroxidase 3	Gpx3	AK002262	Antioxidant
Down	PR domain containing 8	Prdm8	AK019785	Chromatin regulation
	CYP4A10	Cyp4a10	AK002528	Metabolism
	S-adenosylhomocysteine hydrolase	Ahcy	AK075629	Adenosine metabolism
	Glycine N-methyltransferase	Gnmt	AK007398	Methylation
	CYP2C37	Cyp2c37	AK005017	Metabolism
	Carbonic anhydrase 3	Car3	AK003671	Antioxidant
	ATP synthase γ subunit	Atp5c1	AK007063	ATP synthesis
	NADH dehydrogenase (ubiquinone) 1β subcomplex 8	Ndufb8	AK013516	Electron transport
	Transthyretin	Ttr	AK018701	Negative acute phase protein
	CYP1A2	Cyp1a2	BB610038	Metabolism

Table 2-C. Up and down-regulated genes by Kupffer cell specific exposure to α-particles

	Gene	Symbol	GenBank	Function
Up	Lymphotoxin B receptor	Ltbr	AK078859	Immunity
	Histone 1, H1b	Hist1h1b	AK020117	Chromosome organization
	PHD finger protein 14	Phf14	AK016517	Chromatin regulation
	Stoned B/TFIIA- α/β -like factor	Salf	AK014958	Transcription factor, membrane traficking
	Nuclear transcription factor-Y α	Nfya	AK004729	Transcription factor
	UDP-GlcNAc:dolichyl-phosphate N-acetylglucosamine photransferase 1	Dpagt1	AK008246	Protein glycosylation
Down	Nicotinic cholinergic receptor, ε polypeptide	Chrne	AK006411	Neurotransmitter/receptor
	Hairy/enhancer-of-split related with YRPW motif	Heyl	AK004697	Transcriptioin repressor
	3,2 trans-enoyl-CoA isomerase	Dci	AK004838	b-Oxidation of unsaturated fatty acids
	Xeroderma pigmentosum, complementation group C	Xpc	AK004713	DNA repair
	G0/G1 switch gene 2	G0s2	AK003165	G0/G1 transition
	Tubulin, α 4	Tuba4	AK002427	Cytoskeleton
	Nuclear respiratory factor 1	Nrf1	AK014494	Transcription factor
	Acetyl-CoA-acyl transferase 2	Acaa2	AK002555	Fatty acid oxidation
	Insulin-like growth factor binding protein 2	Igfbp2	AK012703	Cell growth regulation

Table 2-D. Up and down-regulated genes by endothel specific exposure to α-particles

	Gene	Symbol	GenBank	Function
Up	Uncoupling protein 1	Ucp1	AK002759	Heat production
	Leucine-rich α-2-glycoprotein1	Lrg1	AK004940	Acute phase protein
	PQ loop repeat containing 1	Pqlc1	AK009256	Electron carrier
	Oxidative-stress responsive 1	Oxsr1	AK075837	Cytoskeleton
Down	BRCA1 associated protein	Brap	AK013885	DNA repair
	Voltage-dependent Ca channel (β2)	Cacnb2	AK020806	Ion channel
	Hemoglobin α adult chain 1	Hba-a1	AK003077	Oxygen delivery
	Acyl-CoA thioesterase 2	Acate2	AK002892	Signal trans., protein traffick

Table 2-E. Up and down-regulated genes by γ-ray exposure

	Gene	Symbol	GenBank	Function
Up	EF hand calcium binding domain 1	Efcab1	AK015426	Ca binding
	Germ cell-less homolog	Gcl	AK004716	Differentiation
	Testis specific gene A2	Tsga2	AK005739	Testis specific
	Membrane-spanning 4-domains, subfamily A, member 8A	Ms4a8a	AK008099	Transporter
	Leucine rich repeat and fibronectin type III domain containing 2	Lrfn2	AK017594	Cell adhesion signal trans.
Down	FK506 binding protein 10	Fkbp10	AK019446	Immunosuppression
	Activating signal cointegrator 1 complex subunit	Ascc3	AK021027	Transcription coactivator
	Secretory carrier membrane protein 1	Scamp1	AK015706	Endocytosis
	Solute carrier family 43, member 1	Slc43a1	AK011417	Transporter

Table 2-F. Up and down-regulated genes by neutron exposure

	Gene	Symbol	GenBank	Function
Up	Diaphanous homolog 1	Diap1	AK012707	Cytoskeleton
Down	Complement receptor related protein	Crry	AK004825	Immunity
	Synaptogyrin 2	Syngr2	AV027954	Synaptic transmission
	Phosphatidylinositol 4-kinase type 2 β	Pi4k2b	AK011751	Inositol lipid biosyhthesis
	M-phase phosphoprotein 9	Mphosph9	AK016065	Cell cycle
	Adenosine kinase	Adk	BB617511	Signal transduction

from the five control non-irradiated mice. Complementary DNA (cDNA) probes were generated starting with 1 µg of polyA RNA using a CyScribe First-Strand cDNA Labelling kit (Amersham Biosciences Corp., Piscataway, NJ). cDNA from irradiated mice was labeled with Cy5 and that from control mice was labeled with Cy3. Pre-hybridization and hybridization were carried out on UltraGAPS coated slides in accordance with the manufacturer's manual (Corning, NY). The image was captured in a GenePix 4000B (Axon Instruments, Inc. CA). The quantification of gene expression arrays was performed by Array Vision software (Imaging Research Inc., Ontario, Canada). Cluster analysis of gene expression was performed by the War method.[8] The experiments were carried out in independent duplicates.

Real-time PCR

In order to validate the results from the microarray analysis we selected 12 genes (Table 1) and compared their gene expression as measured by microarray analysis and real-time PCR. DNaseI treated 500 ng of total RNA was used for the synthesis of cDNA using superscript First-Strand Synthesis System (Invitrogen, Carlsbad, CA). cDNA corresponding to 10 ng of total RNA was amplified using Real-time PCR for the determination of gene expression using QuantiTect SYBR Green PCR Master Mix (QIAGEN K.K., Tokyo, Japan) in an iCycler (BIO-RAD, Hercules, CA). For the normalization of gene expression, a set of primers for β-actin was used.

RESULTS

Compared with non-irradiated controls, mice injected with ^{10}B-liposome solution showed a slight increase in the number and the size of Kupffer cells, indicating that Kupffer cells were irradiated (Kupffer exposure, Fig. 1A). The dilatation of sinusoids was noticed in mice injected with PEG-^{10}B-liposome, indicating sinusoidal endothelial cells were irradiated (Endothelial exposure, Fig. 1B). Liver tissues from mice exposed to γ-rays and neutrons revealed no remarkable histological changes (data not shown). In all cases, parenchymal hepatocytes did not show noticeable changes (Fig. 1).

Table 3. Comparison of gene expressioin levels between microarray and real-time PCR

Symbol	GenBank	endothelial			Kupffer			neutron			gamma		
		Real time-PCR	Micro-Array		Real time-PCR	Micro-Array		Real time-PCR	Micro-Array		Real time-PCR	Micro-Array	
		mean ± S.D.	Mouse 1	Mouse 2	mean ± S.D.	Mouse 1	Mouse 2	mean ± S.D.	Mouse 1	Mouse 2	mean ± S.D.	Mouse 1	Mouse 2
AK3	AK005194	0.66 ± 0.29	0.40	0.45	0.68 ± 0.10	0.29	0.27	0.84 ± 0.28	0.42	0.40	0.95 ± 0.33	0.38	0.48
Atp5b	AK010314	0.52 ± 0.06	0.22	0.44	0.72 ± 0.28	0.35	0.30	0.71 ± 0.17	0.43	0.44	0.90 ± 0.19	0.34	0.45
ATP5c1	AK007063	0.64 ± 0.06	0.27	0.26	0.68 ± 0.07	0.28	0.15	0.83 ± 0.29	0.33	0.28	1.47 ± 0.53	0.91	0.52
Brap	AK013885	0.69 ± 0.14	0.04	0.06	0.89 ± 0.32	0.94	0.13	1.23 ± 0.54	1.66	1.11	2.03 ± 0.71	0.62	0.97
Car3	AK003671	0.07 ± 0.053	0.04	0.20	0.14 ± 0.03	0.26	0.17	0.85 ± 0.27	1.14	1.09	0.53 ± 0.26	0.53	0.74
Egfr	AK004944	1.65 ± 0.84	5.41	4.90	3.39 ± 1.67	5.22	9.07	1.12 ± 0.69	1.68	2.81	1.93 ± 0.81	3.61	1.71
Galnt3	AK019995	0.19 ± 0.05	0.29	0.37	0.39 ± 0.20	0.30	0.34	0.68 ± 0.17	0.43	0.38	0.47 ± 0.06	0.24	0.30
Gsta3	AK014076	0.58 ± 0.14	0.18	0.30	0.85 ± 0.22	0.31	0.30	1.10 ± 0.21	0.46	0.34	0.67 ± 0.10	0.41	0.54
Hpxn	BB610094	36.53 ± 20.07	4.49	6.94	40.33 ± 17.23	6.42	6.38	2.56 ± 1.05	0.61	0.82	8.38 ± 5.3258	6.12	2.90
Lcn2	AK002932	1909.50 ± 558.5	94.79	95.38	1558.30 ± 133.6	34.90	62.41	1.94 ± 1.15	0.79	1.38	6.34 ± 5.20	128.21	-
Mt1	AK018727	24.22 ± 9.13	13.14	16.51	29.51 ± 8.88	15.35	16.38	1.67 ± 0.81	7.20	2.92	15.59 ± 10.66	5.12	4.11
Mt2	AK002567	38.46 ± 25.77	6.47	8.78	42.33 ± 7.71	12.84	19.36	2.57 ± 1.65	2.00	1.37	10.22 ± 7.43	1.99	3.32

Cluster analysis of the microarray results revealed that 2 mice from the same exposure group were the closest, indicating that all the experimental data in this study are reliable (Fig. 2). In this study, only the genes whose over-expression or under-expression compared with non-irradiated control levels which were consistently observed in 2 different mice with the same exposure levels were analyzed. In total, 161 genes were over-expressed by more than 2-fold and 32 genes

Table 4. Comparison of gene expression profiles between radiation exposures and hepatotoxicants

Gene	Symbol	GeneBank	Kupffer cells		Endothel		Neutrons		γ-rays		McMillian *et al.* (rat)	
			Mouse 1	Mouse 2	Mouse 1	Mouse 2	Mouse 1	Mouse 2	Mouse 1	Mouse 2	hepatotoxicants	PPA[a]
Macrophage activation/acute phase response												
Cytochrome P450, family 1, subfamily a, polypeptide 2	Cyp1a2	BB610038	0.32	0.30	0.07	0.15	1.47	1.07	0.63	0.89	0.51	
CYP2C37	Cyp2c37	AK005017	0.23	0.20	0.21	0.23	1.35	1.36	0.60	1.11	0.63	
Fatty acid binding protein 5, epidermal	Fabp5	AK011551	2.85	1.64	1.28	1.76	1.17	1.46	0.71	0.45	2.75	
G-6-phosphatase, transport protein 1	G6pt1	AK003620	0.45	0.43	0.54	0.58	0.70	0.55	0.87	1.39	0.51	0.46
Hemopexin	Hpxn	BB610094	6.41	6.38	4.49	6.94	0.61	0.82	6.12	2.90	1.57	
Insulin-like growth factor binding protein, acid labile subunit	Igfals	AK004926	–	–	–	–	0.32	0.64	1.18	0.52	0.41	
Latent TGF-β binding protein 1	Ltbp1	AK020449	0.41	0.01	0.73	0.08	1.05	0.25	–	0.42	1.06	0.84
Metallothionein 1	Mt1	AK018727	15.35	16.38	13.14	16.51	7.20	2.92	5.12	4.11	1.44	0.23
Pyruvate kinase, muscle	Pkm2	AK002341	1.10	1.23	1.19	1.48	1.00	1.31	1.26	–	2.41	
Retinol binding protein 4, plasma	Rbp4	AK004839	0.32	0.34	0.24	0.40	0.63	0.58	0.61	0.73	0.66	
Superoxide dismutase 2	Sod2	AK002534	1.73	1.77	2.34	1.45	0.76	0.46	1.09	0.96	2.69	
Peroxisome proliferator												
Acetyl-CoA dehydrogenase, medium chain	Acadm	AK008149	0.62	–	0.81	0.87	0.76	0.88	0.52	0.50	0.47	
Brain acyl-CoA hydrolase	Bach	AK010646	1.23	1.25	1.26	1.45	1.06	1.26	0.88	1.02	0.82	2.00
3-hydroxybutyrate dehydrogenase	Bdh	AK009575	0.59	0.66	0.67	0.83	0.76	0.57	0.75	0.54	0.38	
CD36 antigen	Cd36	AK004192	1.20	1.09	1.17	1.15	0.93	1.30	1.10	0.69	1.01	2.87
Dodecenoyl-CoA delta isomerase	Dci	AK004838	0.30	0.10	0.55	0.32	0.54	0.65	0.89	1.10	0.37	1.73
2,4-dienoyl CoA reductase 1	Decr1	AK004725	1.22	1.10	1.11	1.10	1.14	1.22	1.00	0.95	0.45	
Epoxide hydrolase 2	Ephx2	AK002415	0.54	0.55	0.62	0.50	0.99	0.89	0.82	0.75	0.28	
Fatty acid CoA ligase, long chain 2	Facl2	AK004897	0.39	0.32	0.37	0.38	0.68	0.76	0.60	0.73	0.34	
3-hydroxy-3-methylglutaryl-CoA synthase 2	Hmgcs2	AK004865	0.46	0.38	0.48	0.34	1.01	1.21	0.69	1.40	0.44	
ER stress/chaperone protein /HSP												
Annexin A2	Anxa2	AK012563	0.75	1.26	1.45	1.38	1.14	0.93	1.66	–	2.36	
Calreticulin	Calr	AK075605	1.58	1.57	1.35	1.88	0.62	1.21	1.79	1.13	2.28	0.65
Protein disulfide isomerase-related	Pdir	AK012415	1.38	1.35	1.18	0.60	0.94	1.15	0.88	0.58	2.14	0.62
Metabolism												
S-adenosylhomocysteine hydrolase	Ahcy	AK075629	0.21	0.18	0.14	0.26	0.30	0.35	0.42	0.64	0.41	
Betaine-homocysteine methyltransferase	Bhmt	AK016283	1.49	1.70	1.27	1.52	1.20	1.39	1.58	1.99	0.24	
Sulfotransferase family 1A, phenol-preferring, member 1	Sult1a1	AK002700	0.41	0.43	0.35	0.49	0.57	0.59	0.92	0.99	0.43	
Other functions												
G0/G1 switch gene 2	G0s2	AK003165	0.30	0.27	0.48	0.34	0.38	0.36	1.35	2.07	0.60	
Kininogen	Kng	AK005547	1.71	2.65	2.55	2.70	1.37	1.21	1.61	1.04	1.16	0.68
Solute carrier family 34 , member 2	Slc34a2	AK004832	0.45	0.23	0.81	1.78	0.74	1.18	1.24	1.37	1.06	1.59

Light gray background: Under-expressed genes; Black: Over -expressed genes
[a]: Peroxisome proliferator agonist

were over-expressed by more than 3-fold by exposure to either type of radiation. Of the under-expressed genes, 194 showed an expression level of less than 1/2, compared to the control levels and 36 genes showed less than 1/3 compared to the control levels. Approximately the same number of genes showed over-expression of between 2- and 3-fold or under-expression of between a half and a third. Therefore, we defined a gene to be up-regulated when the mean value of its expression levels in exposed mice showed more than a 3-fold over-expression, and down-regulated if its expression level was less than 1/3 compared with non-irradiated mice.

In terms of gene expression profile, Kupffer and endothelial exposures were the most similar to and the neutron exposure group was the most different from other groups (Fig. 2). For commonly up- and down-regulated genes in all the exposure groups, we picked up genes with a level of over-expression of more than 2-fold and under-expression of less than a half among all the radiation groups. Commonly up-regulated genes were metallothionein 1 (Mt1) and protein phosphatase 1, regulatory (inhibitory) subunit 14D (Ppp1r14d). Commonly down-regulated genes were adenylate kinase 3α (Ak3), glutathione S-transferase 3α (Gsta3), ATP (Adenosine triphosphate) synthase β subunit (Atp5b) and UDP (uridine diphosphate)-N-acetyl-α-D-galactosamine-polypeptide (Galnt3) (Fig. 3 and Table 2-A). Commonly up- and down-regulated genes between Kupffer cell irradiation and endothelial cell irradiation are shown in Table 2-B. There were 14 up-regulated genes: 5 associated with cell-cycle regulation, 3 associated with intracellular transportation, 3 that code for metal binding proteins and 3 others. There were 10 down-regulated genes, composed of 3 cytochrome P450 (CYP) genes, 3 associated with ATP synthesis and 4 others. For the genes whose changes in expression were specific to irradiated Kupffer cells, molecules associated with transcription including histone H1 were 3 of 6 up-regulated genes. Of the 9 down-regulated genes, 2 each were respectively associated with cell cycle, transcription and fatty acid metabolism, and 1 was involved in DNA repair (Table 2-C). Among genes specific to endothelial exposure, acute phase protein and cytoskeleton associated gene were up-regulated. Down-regulated genes were associated with signal transduction, protein trafficking and DNA repair (Table 2-D). In contrast to cell specific exposure groups, the genes with altered expression by neutrons or γ-rays were small in number and did not appear to possess significantly different characteristics (Table 2-E and -F). In each Table, up-regulated genes are presented in decreasing order and down-regulated genes in increasing order. All primary Microarray data are available at the site of GEO (http://www.ncbi.nlm.nih.gov/project/geo/) (data No. GSE9290).

In order to validate the consistency of microarray analysis in the present study, we compared gene expression levels of selected genes between microarray and real-time PCR. We determined the mean value of expression of the selected genes in 5 independent mice from each exposure group. This was compared with those in pooled RNA from 5 non-irradiated mice. The qualitative changes in gene expression levels were consistent between these analyses. However, the quantitative difference was greater in real-time PCR than in microarray analysis, both in up- and down-regulated genes (Table 3).

Since radiation exposure could be hepatotoxic, we compared the results of our present study with the results by McMillian *et al.*[9] They performed microarray analysis of gene expression in rat liver 24 hrs after administration of various kinds of hepatotoxic compounds. We picked up genes whose expression level increased more than 2-fold or decreased to less than 1/2 of the control level in their or our study (Table 4). Over-expression of Mt1 and hemopexin (Hpxn), and under-expression of CYP were prominent in radiation-exposed samples compared with those undergoing administration of hepatotoxic chemical compounds and peroxisome proliferator agonists.

DISCUSSION

Gene array analysis of RNA from irradiated tissues is an effective tool for identifying genes of potential interest in the development of tissue injury. Since Thorotrast naturally emits α-particles and causes liver cancers, evaluating changes in gene expression in the liver irradiated with α-particles might help us to understand how Thorotrasts induce liver cancer. In order to analyze the effect of target cell specificity and quality of irradiation on gene expression in the liver, we intended to separately expose Kupffer and endothelial cells to α-particles using BNC, and performed oligonucleotide microarray analysis. Ishida *et al.* reported that 4 hrs after injection into mice, 5% of bare liposomes and 50% of PEG-liposomes are retained in the blood, respectively, whereas, 70% of bare liposomes and 15% of PEG-liposomes accumulate in the liver, respectively.[10] Assuming that liposomes in either form are phagocytosed by Kupffer cells in the liver, the dose ratio of Kupffer group to endothelial group is 4.7 folds in Kupffer cell group and 1/10 in endothelial cell group in this study. Although we could not completely separate target cells for α-particle exposure, we think these numbers were satisfactory because of internal exposure experiments of the mouse. The cellular responses of Kupffer and endothelial groups were the closest to other groups, whilst the group exposed to neutrons showed greatest variations from other groups (Fig. 2). This suggests that cellular responses are mainly determined by the quality of radiation, that is, dependent on exposure to high LET particles or low LET photons.

Acute phase response refers to changes in concentrations of a number of plasma proteins, termed acute-phase proteins (APPs) which reflect re-orchestration of the pattern of gene

expression in hepatocytes in response to a variety of systemic injuries. An APP has been defined as one whose plasma concentration increases (positive APP) or decreases (negative APP) by at least 25% after injury. In the present study, we detected significant changes of the level of APPs such as Hpxn, ceruloplasmin (Cp) and transthyretin (Ttr) commonly in Kupffer and endothelial exposures (Table 2-B). These indicate that the alterations of gene expression in this study reflect those of hepatocytes even after Kupffer cells and endothelial cells were specifically exposed to α-particles. Cp has a scavenger activity[11] and Hpxn acts as an antioxidant by its strong heme binding and iron homeostasis properties.[12] During inflammation, macrophages and endothelial cells secrete the so-called pro-inflammatory cytokines, tumor necrosis factor-α (TNF-α), Interleukin-1β (IL1β) and IL6.[13] Mt also has antioxidant activity and this gene expression is induced by IL6.[14] Lipocalin is also an APP involved in a mammalian defense mechanism against bacterial infection and works by binding to the iron group within bacterial iron-containing siderophores.[15] Interestingly, acute lung injury in mice induced by lipopolysaccharide and diesel exhaust[16] particles up-regulates lipocalin 2 and Mt2 gene expressions.[16] The present study suggests that pro-inflammatory cytokines are secreted by irradiated macrophages and endothelial cells, especially those exposed to α-particles. Mouse macrophages are activated after whole body irradiation to 4 Gy of γ-rays. However, this activation is not a direct effect of radiation but an indirect effect induced by phagocytosis of apoptotic cells after irradiation.[17] In the present study, the destruction of macrophages and endothelial cells in the spleen was also observed (data not shown). We need to take account of the indirect effects on the spleen of radiation exposure when considering liver carcinogenesis of Thorotrast patients, because the spleen in Thorotrast patients is drastically reduced in size compared to the liver. The changes in gene expression profile commonly observed after Kupffer cell and endothelial cell exposures revealed that hepatocytes are in the state of inflammation and are tending towards proliferation at the cost of metabolic activities. Hepatocytes also actively perform quality control of substances by up-regulation of intracellular protein trafficking.

Expression of genes encoding molecules associated with transcription was up-regulated and expression for those associated with signal transduction was down-regulated in the liver. Further study to characterize molecules involved in these gene expressions would elucidate radiation carcinogenesis, especially that of Thorotrast-induced liver tumors. It is noticeable that *epidermal growth factor receptor* (*EGFR*) and *cyclin E1* gene expressions were up-regulated in the liver whose Kupffer cells or endothelial cells were exposed to α-particles, whereas *xeroderma pigmentosum, complementation group C (XPC)* and *insulin-like growth factor binding protein 2 (IGFBP2)* gene expressions were down-regulated in Kupffer cell irradiated group and *BRAP* gene expression in endothelial cell irradiated group. The level of *EGFR* gene expression in tumors has been correlated to the degree of radiation resistance.[18] Exposure of the breast cancer cell line, MCF-7 to γ-rays enhanced EGFR gene expression concomitant with overexpression of its ligand, TGFα,[19] resulting in enhanced cell growth by irradiation.[20] Recently, new targets for cancer treatment have been identified in head and neck squamous cell carcinomas (HNSCC) as playing key roles in tumor proliferation and metastasis. The first one led to the approval of a molecularly based therapy in HNSCC is EGFR.[21] Cyclin E initiates cells to pass from G1- to S-phase and controls genomic stability. High level expression of cyclin E has been associated with the initiation or progression of various human cancers.[22] Transgenic mice in which cyclin E is constitutively expressed develop malignant diseases, supporting the notion of cyclin E as a dominant onco-protein.[23] XPC carries out the first step of global genome repair in nucleotide excision repair. The lack of the XPC protein is associated with UV-induced skin tumors but not with hypersensitivity against ionizing radiation.[24] IGFBP2 in breast cancer cell lines is a marker of resistance against anti-estrogen therapy.[25] It has also been shown that IGFBP2 plays a key role in the activation of the Akt pathway and collaborates with K-Ras or platelet-derived growth factor beta polypeptide (PDGFB) in the development and progression of two major types of glioma.[26] These results suggest that irradiated liver is in the condition toward cancer induction.

Comparison with the data of McMillian *et al.*[9] revealed that all types of radiation exposure investigated involve macrophage activation rather than peroxisome proliferation (Table 4). Up-regulations of Mt1 and Hpxn, and down-regulation of CYP and retinol binding protein 4 (Rbp4) are characteristic of radiation exposure. Steatohepatitis including alcoholic fatty liver is well known to be a precursor status toward liver fibrosis and liver cancer. Since diverse causes of steatohepatitis are characterized by increased mitochondrial (mt) reactive oxygen species (ROS) production, limited repair of mtDNA and accumulation of oxidatively damaged DNA,[27] cellular reaction against radiation toward lipogenesis may indirectly contribute to DNA insult by high LET radiation. Therefore, intensive or preventive anti-inflammatory treatment could help radiation-induced injury. Most of the genes involved in ATP synthesis, oxidative phosphorylation, copper ion homeostasis and electron transport were induced by both continuous and acute exposure of *Saccharomyces cerevisiae* to γ-rays.[28] The results were concordant with the present study though we focused on *in vivo* radiation of the mouse liver. Furthermore, it has been shown that microvascular endothelial cells are the primary target to initiate intestinal radiation damage.[29] These similarities indicate that cell-to-cell interaction in response to radiation *in vivo* is the result of amplification of *in vitro*

signals. In order to separate the effects of irradiation on parenchymal, Kupffere and endothelial cells, experiments involving irradiation of these cell types after cell fractionation are underway in our laboratory.

ACKNOWLEDGEMENTS

This study was supported in part by the Grants-in Aid from the Ministry of Education, Science, Sports and Culture and the Ministry of Health, Labor and Welfare of Japan. We thank Shoko Ono for her technical assistance.

REFERENCES

1. Goto, A., Takebayashi, Y., Liu, D., Li, L., Saiga, T., Mori, T., Yamadera, A. and Fukumoto, M. (2002) Microdistribution of alpha particles in pathological sections of tissues from thorotrast patients detected by imaging plate autoradiography. Radiat Res. **158**: 54–60.
2. Sharp, G. B. (2002) The relationship between internally deposited alpha-particle radiation and subsite-specific liver cancer and liver cirrhosis: an analysis of published data. J Radiat Res. **43**: 371–380.
3. Ober, S., Zerban, H., Spiethoff, A., Wegener, K., Schwarz, M. and Bannasch, P. (1994) Preneoplastic foci of altered hepatocytes induced in rats by irradiation with alpha-particles of Thorotrast and neutrons. Cancer Lett. **83**: 81–88.
4. Kopp-Schneider, A., Haertel, T., Burkholder, I., Bannasch, P., Wesch, H., Groos, J. and Heeger, S. (2006) Investigating the formation and growth of alpha-particle radiation-induced foci of altered hepatocytes: a model-based approach. Radiat Res. **166**: 422–430.
5. Yuda, T., Pongpaibul, Y., Maruyama, K. and Iwatsuru, M. (1999) Activity of Amphipathic Polyethyleneglycols to Prolong the Circulation Time of Liposomes. Journal of Pharmaceutical Science and Technology, Japan. **59**: 32–42.
6. Weichselbaum, R. R., Hallahan, D. E., Sukhatme, V., Dritschilo, A., Sherman, M. L. and Kufe, D. W. (1991) Biological consequences of gene regulation after ionizing radiation exposure. J Natl Cancer Inst. **83**: 480–484.
7. Maruyama, K., Ishida, O., Kasaoka, S., Takizawa, T., Utoguchi, N., Shinohara, A., Chiba, M., Kobayashi, H., Eriguchi, M. and Yanagie, H. (2004) Intracellular targeting of sodium mercaptoundecahydrododecaborate (BSH) to solid tumors by transferrin-PEG liposomes, for boron neutron-capture therapy (BNCT). J Control Release. **98**: 195–207.
8. Ward, J. H., (1963) Hierarchical Grouping to Optimize an Objective Function. J. Am. Statist. Assoc. **58**: 236–244.
9. McMillian, M., Nie, A. Y., Parker, J. B., Leone, A., Kemmerer, M., Bryant, S., Herlich, J., Yieh, L., Bittner, A., Liu, X., Wan, J. and Johnson, M. D. (2004) Inverse gene expression patterns for macrophage activating hepatotoxicants and peroxisome proliferators in rat liver. Biochem Pharmacol. **67**: 2141–2165.
10. Ishida, O., Maruyama, K., Sasaki, K. and Iwatsuru, M. (1999) Size-dependent extravasation and interstitial localization of polyethyleneglycol liposomes in solid tumor-bearing mice. Int J Pharm. **190**: 49–56.
11. Goldstein, I. M., Kaplan, H. B., Edelson, H. S. and Weissmann, G. (1982) Ceruloplasmin: an acute phase reactant that scavenges oxygen-derived free radicals. Ann N Y Acad Sci. **389**: 368–379.
12. Delanghe, J. R. and Langlois, M. R. (2001) Hemopexin: a review of biological aspects and the role in laboratory medicine. Clin Chim Acta. **312**: 13–23.
13. Trey, J. E. and Kushner, I. (1995) The acute phase response and the hematopoietic system: the role of cytokines. Crit Rev Oncol Hematol. **21**: 1–18.
14. Davis, S. R. and Cousins, R. J. (2000) Metallothionein expression in animals: a physiological perspective on function. J Nutr. **130**: 1085–1088.
15. Flo, T. H., Smith, K. D., Sato, S., Rodriguez, D. J., Holmes, M. A., Strong, R. K., Akira, S. and Aderem, A. (2004) Lipocalin 2 mediates an innate immune response to bacterial infection by sequestrating iron. Nature. **432**: 917–921.
16. Yanagisawa, R., Takano, H., Inoue, K., Ichinose, T., Yoshida, S., Sadakane, K., Takeda, K., Yoshino, S., Yamaki, K., Kumagai, Y. and Yoshikawa, T. (2004) Complementary DNA microarray analysis in acute lung injury induced by lipopolysaccharide and diesel exhaust particles. Exp Biol Med (Maywood). **229**: 1081–1087.
17. Lorimore, S. A., Coates, P. J., Scobie, G. E., Milne, G. and Wright, E. G. (2001) Inflammatory-type responses after exposure to ionizing radiation *in vivo*: a mechanism for radiation-induced bystander effects? Oncogene. **20**: 7085–7095.
18. Ochs, J. S. (2004) Rationale and clinical basis for combining gefitinib (IRESSA, ZD1839) with radiation therapy for solid tumors. Int J Radiat Oncol Biol Phys. **58**: 941–949.
19. Schmidt-Ullrich, R. K., Valerie, K. C., Chan, W. and McWilliams, D. (1994) Altered expression of epidermal growth factor receptor and estrogen receptor in MCF-7 cells after single and repeated radiation exposures. Int J Radiat Oncol Biol Phys. **29**: 813–819.
20. Hagan, M., Yacoub, A. and Dent, P. (2004) Ionizing radiation causes a dose-dependent release of transforming growth factor alpha *in vitro* from irradiated xenografts and during palliative treatment of hormone-refractory prostate carcinoma. Clin Cancer Res. **10**: 5724–5731.
21. Le Tourneau, C., Faivre, S. and Siu, L. L. (2007) Molecular targeted therapy of head and neck cancer: Review and clinical development challenges. Eur J Cancer.
22. Donnellan, R. and Chetty, R. (1999) Cyclin E in human cancers. Faseb J. **13**: 773–780.
23. Moroy, T. and Geisen, C. (2004) Cyclin E. Int J Biochem Cell Biol. **36**: 1424–1439.
24. Arlett, C. F., Plowman, P. N., Rogers, P. B., Parris, C. N., Abbaszadeh, F., Green, M. H., McMillan, T. J., Bush, C., Foray, N. and Lehmann, A. R. (2006) Clinical and cellular ionizing radiation sensitivity in a patient with xeroderma pigmentosum. Br J Radiol. **79**: 510–517.
25. Juncker-Jensen, A., Lykkesfeldt, A. E., Worm, J., Ralfkiaer, U., Espelund, U. and Jepsen, J. S. (2006) Insulin-like growth factor binding protein 2 is a marker for antiestrogen resistant human breast cancer cell lines but is not a major growth regulator. Growth Horm IGF Res. **16**: 224–239.

26. Dunlap, S. M., Celestino, J., Wang, H., Jiang, R., Holland, E. C., Fuller, G. N. and Zhang, W. (2007) Insulin-like growth factor binding protein 2 promotes glioma development and progression. Proc Natl Acad Sci USA. **104**: 11736–11741.
27. Gao, D., Wei, C., Chen, L., Huang, J., Yang, S. and Diehl, A. M. (2004) Oxidative DNA damage and DNA repair enzyme expression are inversely related in murine models of fatty liver disease. Am J Physiol Gastrointest Liver Physiol. **287**: G1070–1077.
28. Mercier, G., Berthault, N., Mary, J., Peyre, J., Antoniadis, A., Comet, J. P., Cornuejols, A., Froidevaux, C. and Dutreix, M. (2004) Biological detection of low radiation doses by combining results of two microarray analysis methods. Nucleic Acids Res. **32**: e12.
29. Paris, F., Fuks, Z., Kang, A., Capodieci, P., Juan, G., Ehleiter, D., Haimovitz-Friedman, A., Cordon-Cardo, C. and Kolesnick, R. (2001) Endothelial apoptosis as the primary lesion initiating intestinal radiation damage in mice. Science. **293**: 293–297.

Received on August 16, 2007
Revision received on October 11, 2007
Accepted on October 18, 2007
J-STAGE Advance Publication Date: November 30, 2007

Molecular and Cellular Biochemistry 299: 99–107, 2007.
DOI: 10.1007/s11010-005-9050-1
© Springer 2005

Enhanced expression of adipocyte-type fatty acid binding protein in murine lymphocytes in response to dexamethasone treatment

Soha Abdelkawi Abdelwahab,[1] Yuji Owada,[1] Noriko Kitanaka,[1,3] Anne Adida,[4] Hiroyuki Sakagami,[1] Masao Ono,[2] Makoto Watanabe,[3] Friedrich Spener[4] and Hisatake Kondo[1]

[1]*Division of Histology, Department of Cell Biology, Graduate School of Medical Science, Tohoku University, Sendai 980-8575, Japan;* [2]*Department of Pathology, Graduate School of Medical Science, Tohoku University, Japan;* [3]*Department of Aging and Geriatric Dentistry, Graduate School of Dentistry, Tohoku University, Sendai 980-8575, Japan;* [4]*Department of Biochemistry, University of Muenster, Muenster 48149, Germany*

Published online: 17 November 2006

Abstract

Fatty acids have a great influence on the process of lymphocyte apoptosis which is considered as a modulating factor of immune response in both humans and animals. However the mechanism underlying the function of fatty acids in the process of lymphocyte apoptosis is not fully understood. In this study we show that the appearance of adipocyte-type fatty acid binding protein (A-FABP) is induced upon administration of dexamethasone (DEX) in both *in vivo* and cultured lymphocytes, and its distinct nuclear localization occurs in close relation to the DEX-induced apoptosis process. In immuunohistochemistry of mouse spleen, A-FABP-immunoreactivity starts to occur 3 h after DEX stimulation, and it massively localizes in the nucleus 8 h after the treatment, while no A-FABP-immunoreactivity is discerned in the lymphocytes of normal as well as 24 h post-injection spleen. In the murine T-cell leukemia CTLL-2 cells, A-FABP-immunoreactivity is also induced in both of the cytoplasm and nucleus when the apoptosis is induced by IL-2 retrieval together with DEX treatment, while in the presence of IL-2 A-FABP-immunoreactivity is confined to the cytoplasm with DEX trreatment. On the other hand, A-FABP-immunoreactivity is not detected by IL-2 retrieval alone. The present findings altogether suggest that A-FABP and its ligands, fatty acids, play an important role in the process of apoptosis and the immune modulation induced by DEX. (Mol Cell Biochem **299:** 99–107, 2007)

Key words: fatty acid binding protein, lymphocyte, apoptosis, dexamethazone

Introduction

The apoptosis is a crucial mechanism for regulating immune and inflammatory responses. There has been accumulated evidence for effects of long chain fatty acids on the apoptosis of cultured cells [1]:. Palmitic and arachidonic acids induce the apoptosis *via* induction of the mitochondrial permeability transition [2], palmitic and stearic acids induce apoptosis by *de novo* synthesis of ceramide [3]; and eicosapentaenoic acid induces the apoptosis in human monocytic cells [4], while docosahexaenoic acid markedly reduces the apoptotic effects induced by tumor necrosis factor [5]. In addition, it has been

Address for offprints: Y. Owada, Division of Histology, Department of Cell Biology, Graduate School of Medical Science, Tohoku Univeristy, 2-1 Seiryo-cho, Aoba-ku, Sendai 980-8575, Japan (E-mail: yowada@mail.tains.tohoku.ac.jp)

shown that dietary n-3 polyunsaturated fatty acids attenuate T cell immune-mediated inflammatory diseases and increase the susceptibility to activation-induced cell death in T cells [6]. However, little information is available on the molecular mechanisms underlying the effects of long chain fatty acids on apoptosis.

Fatty acids are hardly soluble in the aqueous cytoplasmic environment; therefore they are solubilized and transported intracellularly to different cellular organelles or proteins by specific lipid binding proteins (LBPs). Multiple species of intracellular lipid binding proteins have been classified into 4 subfamilies based on the phylogenetic relationship and on the structure and conformation of bound ligands, among which five species of fatty acid binding proteins (FABPs), i.e. adipocyte-type (A-), brain-type (B-), epidermal-type (E-) and heart-type (H-) species bind specifically to long chain fatty acids. Thus it is highly possible that these FABPs are involved in the fatty acid-mediated apoptotic process *via* shuttling their lignds within cells. We have recently shown that E-FABP-immunoreactivity is selectively localized in the dendritic cells of the splenic white pulp of mice, and further that apoptotic splenic lymphocytes *in situ* induced by lipopolysaccharide (LPS) are phagocytosed by the dendritic cells which are labeled with E-FABP-immunoreactivity [7]. These findings suggest that E-FABP and/or its ligands, fatty acids, play an important role in the immune modulation *via* the antigen-presentation and/or phagocytosis of apoptotic splenic lymphocytes by the dendritic cells. However, there has so far been no information about which type of FABP is expressed in apoptotic lymophocytes themselves of the spleen. Therefore, for understanding the molecular mechanism of fatty acids on the apoptosis, it is crucial to identify FABPs in splenic lymphocytes under apoptosis because the altered control of apoptosis may result in the cancer or autoimmunity [8].

The present study, as one of series of our studies on FABPs [7, 9–13], was attempted to answer this question. The result shows a selective and transient appearance of A-FABP among FABPs in splenic lymphocytes *in situ* after systemic administration of dexamethasone (DEX) and also in murine T-cell leukemia cells CTLL-2 treated with DEX, both of which have been shown to be models for DEX-induced apoptosis of lymphocytes [14–16]. The functional significance of the present transient appearance of A-FABP in the apoptotic cell nuclei of lymphocytes was discussed in relation to possible involvement of A-FABP in the regulation of transcription in the nucleus *via* PPARγ, based on previous findings that A-FABP is translocated from the cytosol to the nucleus of lymphocytes upon activation by ligands of peroxisome proliferatore activated receptor γ (PPARγ) [17] and that its activation results in apoptosis of lymphocytes [18, 19].

Materials and methods

Animals and cells

Male mice of C57BL/6 strain at stages of postnatal 6 week were used in this study. They were maintained in normal laboratory condition. All experimental protocols were reviewed by the Committee on the Ethics of Animal Experiments of Tohoku University, and were carried out in accordance with the Guidelines for Animal Experiments issued by Graduate School of Medicine, Tohoku University. Murine T-cell leukemia CTLL-2 cells was a gift from Dr. N Ishii, Department of Immunology, Tohoku University School of Medicine, and maintained in RPMI1640 containing 10% fetal bovine serum in the presence of murine IL-2 (50 U/mL) under humid atmosphere at 37 °C and 5% CO_2 condition.

Induction of apoptosis by DEX

For the administration of DEX to the mice, 200 μg of DEX (dexamethasone 21-phosphate; SIGMA, USA) dissolved in 500 μl of saline was injected intraperitoneally. Three mice were sacrificed under ether anesthesia at each stage of the postinjection 0, 3, 8 and 24 h, and spleens were rapidly removed and snap-frozen for analyses of RT-PCR and Western blot, or transcardially perfused by 4% paraformaldehyde/0.1 M phosphate buffer for immunohistochemistry and *in situ* hybridization. CTLL-2 cells were plated in 35 mm tissue culture dishes (Nalge Nunc International, USA) at 1×10^6 cells/dish in RPMI1640/10%FCS medium in the absence or presence of IL-2 (50 U/ml), and 20 μM of DEX dissolved in RPMI1640 medium was applied to each dish. The cells at each stage of 0, 3, 8 and 24 h following DEX treatment were fixed with 4% paraformaldehyde/0.1 M phosphate buffer for immunocytochemistry, or frozen for RT-PCR and Western blot analysis.

Antibodies against FABPs

Murine A-FABP was expressed in fusion with an N-terminal 6× histidine tag (His-tag). Competent BL21(DE3)pLysS *E. coli* cells were transformed with murine A-FABP cDNA [20] cloned into the pET15b expression vector (Novagen). The cells were grown in LB medium at 37 °C to $A_{600} = 0.4$–0.8 and protein expression was induced by addition of 1 mM IPTG to the medium. After further growth at 30 °C for 2.5 h, cells were centrifuged and the pellet was kept overnight at −80 °C, resuspended in a lysis buffer (50 mM NaH_2PO_4 pH 8.0, 300 mM NaCl, 10 mM imidazole) and incubated with 25 U benzonase/ml extract for 20 min at 37 °C. After

sonication, the extract was centrifuged for 10 min at 28000g, the supernatant treated with 1.5% (w/v) streptomycine sulfate for 30 min at 4 °C and subsequently centrifuged for 60 min at 28000g. His-tagged A-FABP was purified upon application of the supernatant to a Ni-NTA Superflow column (QIAGEN, Germany) and eluted with a lysis buffer containing first 20 mM, then 250 mM imidazole. For antibody production, rabbits (white New Zealand) were immunized with 400 μg purified recombinant A-FABP and boosted after four weeks with 200 μg A-FABP. Polyclonal antibodies were purified by affinity chromatography using purified A-FABP coupled to CH-activated Sepharose 4B (Amersham Biosciences) according to the manufacturer's instructions. Bound antibodies were eluted with a solution composed of 10 mM sodium citrate and 20 mM sodium phosphate (pH 2.8), and immediately neutralised with a 0.5 M phosphate buffer (pH 7.4).

The specificities of antibodies against H-, B- and E-FABPs have previously been reported elsewhere [21].

Histochemical analysis

For immmunohistochemistry, spleens were extirpated and immersed overnight in a phosphate buffer containing 30% sucrose after perfusion fixation with a fixative of 4% paraformaldehyde/0.1 M phosphate buffer. Sections, 20 μm in thickness, were prepared on a cryostat. For immunocytochemistry of CTLL-2 cells, cells were attached onto glass slides using a centrifugal cell collector (TOMY SEIKO, Japan). The sections were incubated with rabbit anti-murine antibodies againt A-, H-, B- and E-FABPs at a concentration of 0.5 μg/ml for 12 h at 4 °C. After incubation with the primary antibody, the sections were incubated with biotinylated secondary antibody or with anti-rabbit antibody labeled by Alexa488 (Molecular Probe, USA). For the peroxidase method, sections were subsequently visualized using ABC (avidin-biotinylated peroxidase complex) system (Vector Laboratory, USA) with DAB as a substrate. For TUNEL (terminal deoxynucleotidyl transferase-mediated deoxyuridyl triphosphate nick end labeling) combined with A-FABP immunohistochemistry, cryosections of spleen were incubated in the solution containing 100 mM sodium cacodylate (pH 7.0), 1 mM $CoCl_2$, 50 μg/ml gelatin, 10 nM/ml biotin-16-dUTP (Roche, Germany) and 100 U terminal deoxynucleotidyl transferase (Takara, Japan). After several washes with TPBS (0.1% Tween/phosphate buffered saline), sections were incubated with A-FABP antiserum followed by incubation with anti-rabbit IgG-Alexa488 (Molecular Probe, USA) and anti-biotin IgG-Alexa594 (Molecular Probe, USA). The sections were mounted with Vectashield containing DAPI (Vector, USA), and observed by confocal laser microscope (Leica, Germany).

For immuno-electron microscopy, some of the sections were postfixed with 1% OsO4 in 0.1% cacodylate buffer (pH 7.4) for 20 min after completion of the ABC procedure. They were embedded in Epon according to the conventional procedure and ultrathin sections were examined after brief staining with uranyl acetate.

The procedure of *in situ* hybridization was described previously [22]. For preparation of digoxigenin(DIG)-labeled cRNA probe complementary to murine A-FABP, the plasmid containing murine A-FABP cDNA [20] was linearized with Nco1 (for antisense probe) or with Spe1 (for sense probe). The RNA transcription was performed using a DIG-RNA labeling kit (Roche, Germany) according to the manufacture's manual. The concentration of the labeled probes was determined by dot-spot methods. 4% paraformaldehyde fixed sections of 20 μm thickness were prepared by a cryostat. The sections were acetylated, dehydrated and hybridized with labeled antisense or sense cRNA probe for mouse A-FABP cDNA. After several wash, anti-DIG antibody conjugated with alkaline phosphatase (Roche Diagnostics, Germany) were applied to the sections and signals were developed by DIG detection kit (Roche Diagnostics, Germany). The specificity of the probe was tested using mouse adipose tissue as positive control, where hybridization signals appeared only upon applying anti-sense probe, while no hybridization signals could be detected with sense probe (data not shown).

RT-PCR

For reverse transcription PCR (RT-PCR) analysis, total RNA was isolated using the guanidine isothiocyanate based TRIzol solution (GIBCO-BRL, Burlington, ON, Canada) according to the manufacturer's manual. Single strand cDNAs were reverse-transcripted from the separated total RNA using Reverse Transcription System (Promega, USA). Semiquantitative PCR analyses on the synthesized cDNA from the cells were performed to amplify the transcript of A-FABP, and GAPDH was used as an internal standard. The nucleotide sequences of the primers for A-FABP were as follows: 5′-TCAACCTGGAAGACAGCTCCT-3′ for the sense primer and 5′-TCGACTTTCCATCCCACTTC-3′ for the anti-sense primer. Polymerase chain reaction was performed on a GeneAmp PCR system 9700 (Applied Biosystems, Foster, CA USA) using 100 ng of cDNA, 5 pmol of each oligonucleotide primer, 200 μM of dNTP, 1 unit of taq polymerase (Takara, Tokyo, Japan) and 1× PCR buffer (Takara, Tokyo, Japan). PCR program was initially started with 94 °C denaturation for 4 min followed by 25 cycles and 28 cycles of 94 °C/1 min, 60 °C/1 min, 72 °C/1 min for GAPDH and A-FABP gene, respectively. Linear amplification of the band was confirmed in advance for A-FABP gene in this condition. PCR products were electrophoresed on 1.5% agarose gel and gel images

were digitally captured by ChemiDoc XRS (Bio-Rad Laboratories, Hercules, CA, USA) and the density of the amplified band was measured by the Quantity One software (Bio-Rad Laboratories, Hercules, CA, USA). The values were presented as a ratio of specified gene signal density divided by that of GAPDH.

Western blotting

In Western blotting, cytosolic and nuclear fractions of the CTLL-2 before and 24 h after the DEX treatments were prepared using NE-PER Nuclear and Cytoplasmic Extraction Reagents (PIERCE, USA). The concentrations of extracted proteins were determined by a BCA kit (PIERCE, USA), and 25 μg of each samples were loaded onto 12% SDS-PAGE gel under reducing conditions and the gel was electro-blotted onto a PVDF membrane (GE Osmonics, USA). The membrane was incubated with rabbit polyclonal anti-A-FABP antibody at a concentration of 2 μg/ml in PBS (pH7.4) containing 0.1% Tween 20. After incubation of the membrane with horseradish peroxidase-conjugated anti-rabbit IgG, the immunopositive band was visualized by ECL plus Western blot detection system (Roche, Germany). Gel images were digitally captured by ChemiDoc XRS (Bio-Rad Laboratories, USA) and the density of positive bands was measured by the Quantity One software (Bio-Rad Laboratories, USA). The values were presented as a ratio of specified band density divided by that of β-actin.

Results

The quality of the A-FABP antibody was checked by Western blotting, in which the antibody was able to detect A-FABP (14.6 kDa) in extracts of 3T3-L1 adipocytes and of QT6 fibroblasts transfected with 3 μg or 6 μg of pCDNA3 expressing A-FABP, but not in QT-6 cells transfected only with empty pCDNA3 (Fig. 1). Cross-reactivity of the antibody with other FABP paralogs was tested by dot blotting (data not shown). A weak cross-reaction was observed with B- and H-FABP with signals more than 10-fold lower than that for A-FABP in the densitometer analysis. No cross-reactivity was observed with E- and L-FABP.

Expression and localization of A-FABP in in vivo spleen after DEX administration

By immunohistochemistry, A-FABP-immunoreactivity was detected only in the endothelial cells of capillaries and arterioles surrounding individual white pulps, and no significant immunoreactivity was seen within both of the white and red

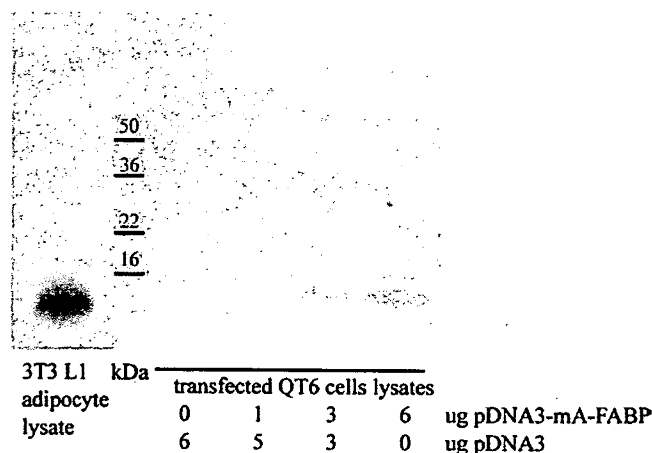

Fig. 1. Characterization of anti-murine A-FABP antibody. The antibody was able to detect A-FABP (14.6 kDa) in extracts of 3T3-L1 adipocytes and of QT6 fibroblasts transfected with 3 μg or 6 μg of pCDNA3 containing murine A-FABP cDNA (pCDNA3-mA-FABP), but not in QT-6 cells transfected only with empty pCDNA3.

pulps in the spleen of adult mice without any extrinsic stimuli (Fig. 2C). At 3 h after injection of DEX, small aggregations of round cells showing the distinct immunoreactivity for A-FABP were distributed randomly without any specific spatial relation to the central arterioles throughout the white pulps (Fig. 2D). At 8 h postinjection, the immunopositive cell aggregations were more numerous and larger than the previous stage and they were composed of 5–10 immunopositive cells versus 1–3 cells at the previous stage (Fig. 2E and 2G). The intense immunopositivity appeared as round profiles representing the nuclei as well as the cytoplasm or as ring profiles with pale round cores, representing the cytoplasmic rim, with the former profiles much more numerous (Fig. 2G). The immunopositive structures seemed to be smaller in diameter than the adjacent immunonegative cells. At 24 h postinjection, A-FABP-immunopositivity was almost close to the background in any portions of the white pulps (Fig. 2F). The immunopositivity in the endothelial cells of vessels surrounding the white pulps remained unchanged during the course examined and no nuclear accumulation of A-FABP-immunoreactivity was seen in the cells. When the specimens were processed simultaneously for TUNEL reaction and A-FABP immunostaining, almost all cell profiles intensely immunopositive for A-FABP in immunolight microscopy were co-stained for TUNEL-reaction in spleen at 3 and 8 h postinjection (Fig. 2H). When sections of the spleens were reacted with the control serum in which the antibody was pre-absorbed with the recombinant murine A-FABP, no significant immunoreaction was discerned in any portions of the sections, indicating that the immunoreaction described above was due to authentic A-FABP (data not shown). When the antibodies against H- and B-FABPs were applied to sections of

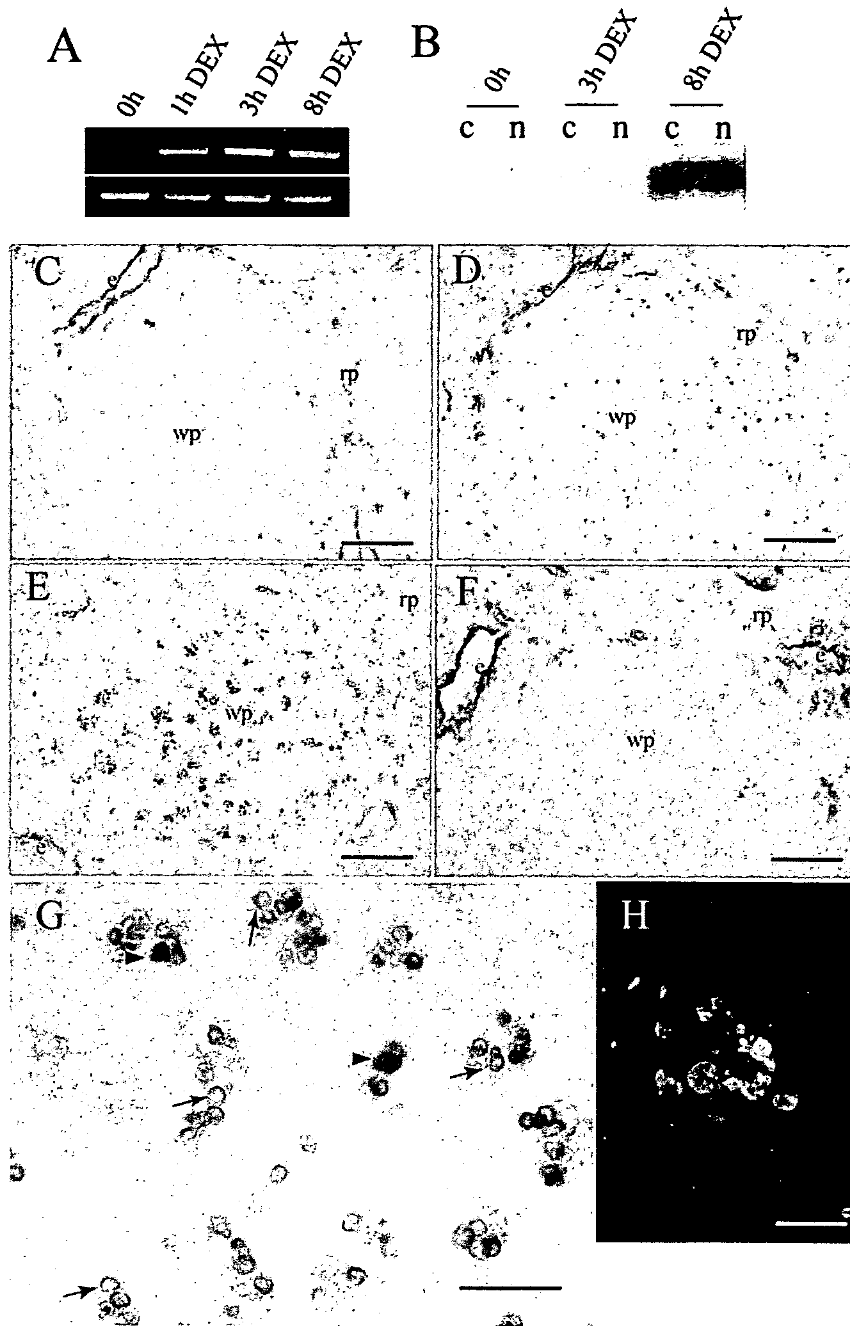

Fig. 2. Enhanced expression of A-FABP in the mouse spleen after DEX treatment. (A) RT-PCR analysis shows that the amplified band was markedly increased in density at 1, 3 and 8 h postinjection of DEX. GAPDH mRNA expression is shown in the lower lane as an internal standard. (B) Western blot analysis of cytosolic (c) and nuclear (n) protein fractions from the spleen, showing the progressive increase of A-FABP protein synthesis at 3 and 8 h after DEX treatment in both cytosol and nucleus. (C)–(G) Immunolight micrographs showing A-FABP localization before and after DEX treatment. Before DEX treatment, none of the immunopositive cells are discerned in the white pulp (wp) although the immunoreaction is seen in endothelial cells (e) of the red pulp (C). At 3 h after DEX treatment, small aggregations of the immunopositive cells are seen randomly throughout the white pulp (D) and the cell aggregations are more increased at 8 h after the treatment (E). At 24 h after the treatment, immunopositive cells are not detected in the white pulp (F). At higher magnification of the white pulp at 8 h after the treatment, immunopositive cells for A-FABP with ring (arrows) and round (arrow heads) profiles are detected (G). (I) Double immuno-fluorescent staining for A-FABP (green) and TUNEL (red), showing that most of A-FABP positive cells were TUNEL positive. wp; white pulp, rp; red pulp. Bars in C–F = 300 μm, bars in G = 50 μm, bar in H = 25 μm.

the same spleens as examined above, no immunoreactivity was detected in any portions of the spleens. When employed the antibodies against E-FABP, the immunoreactivity was found in the dendritic cells of the white pulp and endothelial cells of the red pulp as already reported elsewhere (Kitanaka *et al.*, 2003). Therefore, the subsequent examination in this study was confined to A-FABP, and two time points of postinjection 1 and 8 h were selected as the beginning and maximum stages of the chronological change based on the immunohistochemical finding.

In RT-PCR analysis, the amplified band of A-FABP gene was close to the background level in the spleen of adult mice without any extrinsic stimuli. The amplified band was markedly increased in density at 1 and 8 h postinjection of DEX (Fig. 2A). In Western blot analysis of both cytosolic and nuclear proteins isolated from the spleens before, 3 and 8 h after DEX treatment, a marked increase in the A-FABP protein synthesis was observed in both of the nuclear and cytosolic fractions at 3 and 8 h after DEX treatment (Fig. 2B).

By *in situ* hybridization histochemistry, distinct signals representing mRNA for A-FABP were observed in the splenic white pulp as small aggregations of cell profiles at 3 h postinjection of DEX, while no positive signals were detected throughout the normal spleen (Fig. 3A and 3B). As a negative control, no expression was confirmed in adjacent sections incubated with the sense A-FABP cRNA probe (Fig. 3C).

In immuno-electron microscopy of the 8 h-specimen, immunopositive cells of round contour were grouped together to form cell islets among splenocytes having normal cytological appearance. The immunopositive cells were smaller than adjacent immunonegative splenocytes and the immunoreaction products were present in the cytoplasm. The immunopositive cells contained single or multiple bodies of round or polymorphous contour with a high and homogenous electron density. They were intimately enclosed together by cells having larger and irregular-shaped nucleus poor in chromatin (Fig. 4). Based on the ultrastructural features, the immunopositive round cells and their electron-dense bodies are regarded as apoptotic splenocytes and their nuclei, and the enclosing cells as the dendritic cells.

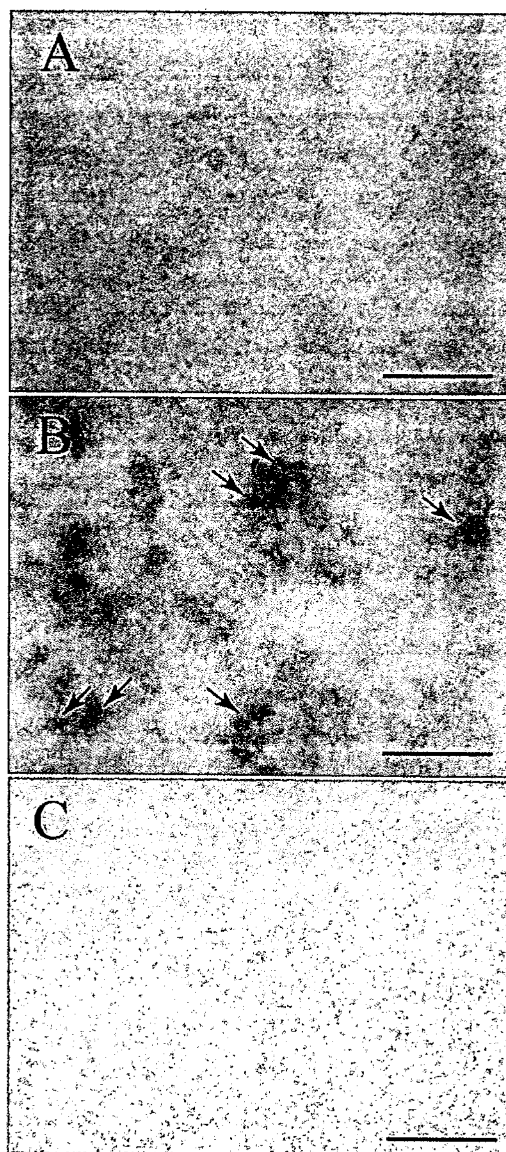

Fig. 3. In situ hybridization histochemistry for A-FABP. A-FABP-positive cells are detected in forms of cell aggregations in the white pulp at 3 h after DEX treatment (B), while the expression signals are observed neither in the pre-treatment spleen (A) nor in the negative- control section (C) probed by sense A-FABP cRNA. Note the similar distribution pattern of A-FABP-positive cells to that of A-FABP immunopositive cells within the white pulp shown in Fig. 2D and E. Bars in A–C = 100 μm.

Expression and localilzation of A-FABP in CTLL-2 cells after DEX treatment

In RT-PCR analysis, an amplified band for A-FABP mRNA was clearly detected in CTLL-2 cells at 1 h after applying DEX into the cultured media although such a band was not discerned before the application. The amplified band increased in density progressively at 3 and 8 h after DEX application, and no significant signals were visible at 24 h after the application (Fig. 5A). In Western blotting of both cytosolic and nuclear fractions isolated from CTLL-2 at stages of 3, 8 and 24 h after DEX application in the absence of IL-2, a band for A-FABP protein was weakly detected only in the cytosolic, but not nuclear, fraction at the 3 h stage, while the band was evident at the stages of 8 h and 24 h in both the nuclear and cytosolic fractions. In the presence of IL-2, a band for A-FABP protein was negative in the nuclear fraction although it was clearly detected in the cytosol as intense as that of the cells under IL-2 deprivation (Fig. 5B).

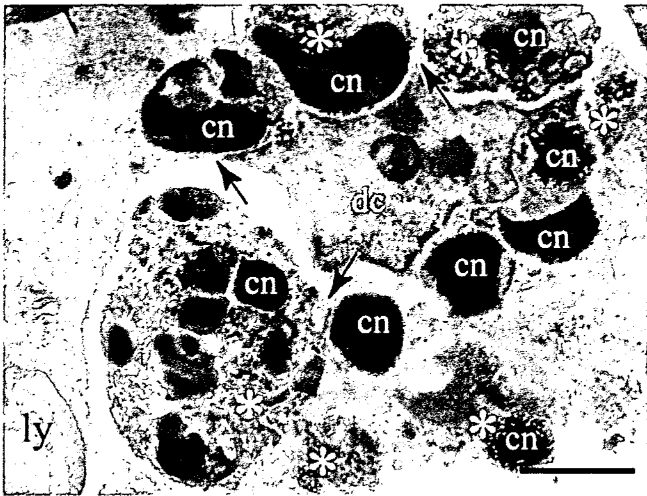

Fig. 4. Immunoelectron micrograph of the spleen 8 h after DEX treatment Immunopositive cells (asterisks) were smaller in size and more electron-dense compared to the adjacent immunonegative lymphocytes (ly), and contained condensed nuclei (cn). Note that the immunopositive cells are enclosed by an immunonegative presumptive dendritic cell (dc). Arrows indicate the cytoplasmic continuity of the immunonegative dendritic cell. Bar = 5 μm.

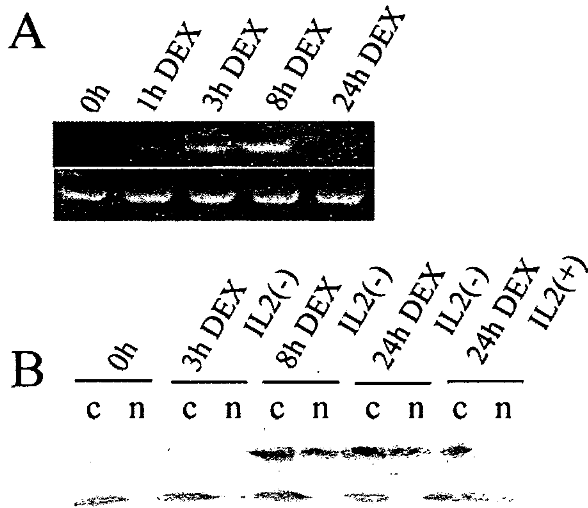

Fig. 5. Enhanced expression of A-FABP in murine CTLL-2 after DEX treatment. (A) In RT-PCR analysis, a marked enhancement of A-FABP gene expression is detected from 3 to 8 h after DEX treatment, and returns to the pretreatment level at 24 h after DEX treatment as shown in the upper lane. GAPDH mRNA expression is shown in the lower lane as an internal standard. (B) Western blot of both cytosolic (c) and nuclear protein (n) fractions from CTLL-2 cells. A distinct band for A-FABP appears only in the cytosol but not in the nuclear fraction at 3 h after DEX(+)IL-2(−) treatment, while the band appears in both the cytosolic and nuclear fractions at 8 and 24 h after the treatment as shown in the upper lane. In the presence of IL-2, a band for A-FABP is detected only in the cytosolic fraction at 24 h after DEX treatment. The bands for β-actin are shown in the lower lane as protein standardization. c; cytosolic protein fraction, n; nuclear protein fraction.

In immunocytochemistry, no cells immunopositive for A-FABP or TUNEL were detected when CTLL-2 cells were maintained in the culture media containing IL-2 without DEX (DEX(−)IL-2(+)) (Fig. 6A). Many cells exhibited A-FABP-immunopositivity in forms of rings containing immunonegative round cores at 3 h after application of DEX into the cultured media without IL-2 (DEX(+)IL-2(−)), although a

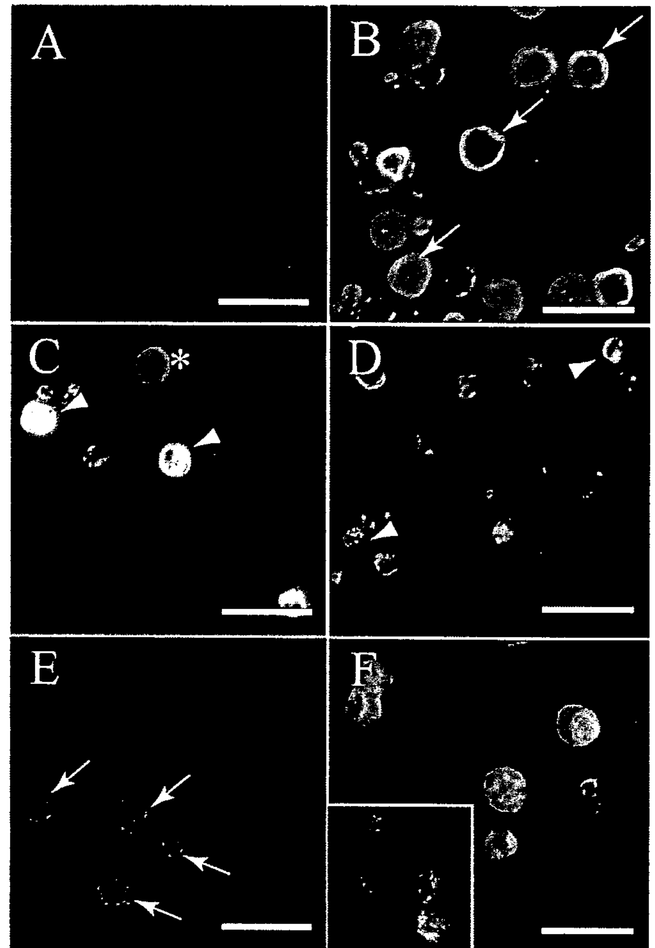

Fig. 6. Immunofluorescence photomicrographs of A-FABP expression (green) and TUNEL reaction (red) in murine CTLL-2 cells. (A) Neither A-FABP expression nor TUNEL reactivity is seen in CTLL-2 cells without DEX-treatment. (B) A-FABP expression is predominately detected in forms of rings (arrows), representing the cytosolic localization at 3 h after DEX treatment. (C) At 8 h after DEX treatment, A-FABP expression is shown in a round pattern superimposed on entire profiles of cells (asterisks). The cell nuclei co-stained by A-FABP and TUNEL are indicated by arrowheads. (D) At 24 h after DEX treatment almost all cells are smaller and deformed in shape, and they are positive for both A-FABP and TUNEL (arrow heads). (E) When the cells are cultured in media containing neither IL-2 nor DEX for 24 h, A-FABP expression is not detected in any cells and about 50% of cells are TUNEL positive (open arrows). (F) In culture media containing both IL-2 and DEX for 8 h (shown in inset) and 24 h, occurrence of A-FABP is confined to the cytosol without any nuclear localization. (A)–(F) Cell nuclei are stained with DAPI (blue). Bars in A–F = 20 μm.

few cells showed the immunopositivity in forms of round profiles representing the entire cell bodies (Fig. 6B). At 8 h after DEX(+)IL-2(−) treatment, many cells were immunopositive for A-FABP, although cells in a unit area in light microscopy were less numerous. Most of the immunopositive cells appeared as round profiles of smaller sizes than those at the previous stage although a few cells exhibiting the immunopositive rings were remained (Fig. 6C). The round cell profiles immunopositive for A-FABP were also positive for TUNEL reaction. At 24 h after DEX(+)IL-2(−) treatment, almost all cells were much smaller and some of them seemed to be deformed more or less. They were positive for both A-FABP and TUNEL. No immunopositive cells in forms of the ring profile were found among them (Fig. 6D). On the other hand, although numerous TUNEL-positive cells were also seen 24 h after DEX(−)IL-2(−) treatment, they were immunonegative for A-FABP (Fig. 6E). Furthermore, numerous cells showed A-FABP-immunopositivity in forms of ring, but not round, profiles at 8 and 24 h after DEX(+)IL-2(+) treatment. However, most of them were TUNEL-negative (Fig. 6F).

Discussion

The present study shows for the first time the appearance of A-FABP in the cytoplasm of a limited population of splenic lymphocytes at early stages of the DEX administration, and its appearance in the nuclei as well as the cytoplasm of numerous apoptotic lymphocytes at its later stage. This finding suggests the enhanced appearance of A-FABP in splenic lymphocytes under the apoptotic process induced by DEX *in vivo* and the translocation of A-FABP into the nuclei as the apoptosis proceeds. The ultrastructure of the immunopositive cells and their enclosed/engulfed feature by immunonegative dendritic cells in *in vivo* spleen may raise question whether or not the positive immunoreaction represents the authentic A-FABP and whether or not its enhancement is due to the increase at the transcription level. In this regard, the expression of A-FABP mRNA examined by *in situ* hybridization histochemistry was localized in the white pulp of the spleen at 3 h postinjection of DEX in a pattern well corresponding to the immunohistochemical results, which is in accord with the time course expression of the mRNA by RT-PCR analysis of the spleen. Furthermore, we found the apoptosis-linked enhancement of expression of A-FABP at levels of both mRNA and protein in the cultured murine lymphocytic cell line, CTTL-2 and the relocation of A-FABP into the nuclei. These findings thus confirm that the synthesis of A-FABP is induced in the cells under DEX-induced apoptosis regardless of being enclosed/engulfed by any phagocytosing cells, and that A-FABP translocates into their nucleus in association with the apoptosis.

There has been evidence that DEX induces the gene expression for A-FABP in both adipocytes and non-adipocytes such as differentiated myogenic C2C12 cell line [23] and J744 macrophage cell line [24]. The induction has been shown to occur in the presence of cyclohexamide, suggesting that DEX does not require the synthesis of any intermediate proteins [23]. In addition, the gene for A-FABP contains a glucocorticoid response element within the upstream regulatory region [25]. Therefore, it is likely that DEX directly enhances A-FABP expression in the present lymphocytes.

The present study also shows that, DEX treatment, in the presence of IL-2 which is known to rescue CTLL-2 cells from apoptosis [16], does not induce the nuclear translocation of A-FABP in the lymphocytes, although its localization is discerned in the cytoplasm. The presence of IL-2 in the culture media has recently been shown to hinder the nuclear translocation of glucocorticoids hormone receptor (GHR) which occurs in the process of apoptosis induced by DEX in murine T cell line [26]. Together with the absence of enhanced appearance of A-FABP under apoptosis induced solely by IL-2 deprivation, the expression and subsequent translocation of A-FABP into apoptotic cell nuclei is specific to the DEX-induced apoptotic signaling pathway. It was shown recently that GHR- and PPAR-dependent signaling have a possible crosstalk in the hepatocytes [27], suggesting that A-FABP-PPAR- and GHR-mediated signaling cascade might cooperatively be involved in the DEX-mediated apoptotic process of lymphocytes.

With regard to the functional significance of enhanced protein synthesis and nuclear translocation of A-FABP under the process of apoptosis, a recent finding on the enhancement of PPARγ activity by A-FABP in COS-7 fibroblast cells and their ligand-dependent direct protein interaction [17] should be noted. It is known that a natural PPARγ ligand 15d-PGJ2, which is also one of ligands of FABPs, induces the apoptosis through direct inhibition of NFκB [28], while IL-2 rescues DEX-induced apoptosis of Th1 cells through activation of NFκB [16]. In addition, PPARγ has been shown to be primarily located in the cytoplasm in naïve T lymphocytes and translocates to the nucleus upon its activation [29]. Furthermore, A-FABP has recently been shown to induce the apoptosis of prostate cancer cells and to regulate the cell proliferation via enhanced TNFα expression, suggesting the involvement of A-FABP in the regulation of gene expression in the apoptotic process [30]. It is thus possible that A-FABP and/or its binding fatty acids are intimately involved in the DEX-induced apoptotic process of lymphocytes in corporation with nuclear transcription factors such as PPARγ *via* inhibition of NFκB, leading to changes in response of lymphocytes to various pathogens or microbes. Indeed, PPARγ ligands have been shown to reduce the systemic inflammation in polymicrobial sepsis *in vivo* [31], and thus A-FABP can be a possible therapeutic target for the modulation of

inflammation. It would be necessary to perform the genetic ablation of A-FABP in the lymphocytes, which should shed more light on a causal relationship between A-FABP and/or its ligand fatty acids and apoptosis.

Acknowledgments

We are grateful to Hiroo Iwasa for his technical assistance in this study. This work was supported by grants from the Ministry of Education, Science, and Culture of Japan, nos. 14370002 and 14657623 (to H.K.) and no. 14580720 (to Y.O.), and a grant from Hiromi Medical Research Foundation to Y.O.

References

1. Rudolph IL, Kelley DS, Klasing KC, Erickson KL: Regulation of cellular differentiation and apoptosis by fatty acids and their metabolites. Nutr Res 21: 381–393, 2001
2. Scorrano L, Penzo D, Petronilli V, Pagano F, Bernardi P: Arachidonic acid causes cell death through the mitochondrial permeability transition. Implications for tumor necrosis factor-alpha aopototic signaling. J Biol Chem 276: 12035–12040, 2001
3. Paumen MB, Ishida Y, Muramatsu M, Yamamoto M, Honjo T: Inhibition of carnitine palmitoyltransferase I augments sphingolipid synthesis and palmitate-induced apoptosis. J Biol Chem 272: 3324–3329, 1997
4. Finstad HS, Drevon CA, Kulseth MA, Synstad AV, Knudsen E, Kolset SO: Cell proliferation, apoptosis and accumulation of lipid droplets in U937-1 cells incubated with eicosapentaenoic acid. Biochem J 336(Pt 2): 451–459, 1998
5. Yano M, Kishida E, Iwasaki M, Kojo S, Masuzawa Y: Docosahexaenoic acid and vitamin E can reduce human monocytic U937 cell apoptosis induced by tumor necrosis factor. J Nutr 130: 1095–1101, 2000
6. Switzer KC, McMurray DN, Morris JS, Chapkin RS: ($n - 3$) Polyunsaturated fatty acids promote activation-induced cell death in murine T lymphocytes. J Nutr 133: 496–503, 2003
7. Kitanaka N, Owada Y, Abdelwahab SA, Iwasa H, Sakagami H, Watanabe M, Spener F, Kondo H: Specific localization of epidermal-type fatty acid binding protein in dendritic cells of splenic white pulp. Histochem Cell Biol 120: 465–473, 2003
8. Thome M, Tschopp J: Regulation of lymphocyte proliferation and death by FLIP. Nat Rev Immunol 1: 50–58, 2001
9. Abdelwahab SA, Owada Y, Kitanaka N, Iwasa H, Sakagami H, Kondo H: Localization of brain-type fatty acid-binding protein in Kupffer cells of mice and its transient decrease in response to lipopolysaccharide. Histochem Cell Biol 119: 469–475, 2003
10. Owada Y, Yoshimoto T, Kondo H: Spatio-temporally differential expression of genes for three members of fatty acid binding proteins in developing and mature rat brains. J Chem Neuroanat 12: 113–122, 1996
11. Owada Y, Suzuki R, Iwasa H, Spener F, Kondo H: Localization of epidermal-type fatty acid binding protein in the thymic epithelial cells of mice. Histochem Cell Biol 117: 55–60, 2002
12. Watanabe M, Ono T, Kondo H: Immunohistochemical studies on the localisation and ontogeny of heart fatty acid binding protein in the rat. J Anat 174: 81–95, 1991
13. Owada Y, Abdelwahab SA, Suzuki R, Iwasa H, Sakagami H, Spener F, Kondo H: Localization of epidermal-type fatty acid binding protein in alveolar macrophages and some alveolar type II epithelial cells in mouse lung. Histochem J 33: 453–457, 2001
14. Iwata M, Ohoka Y, Kuwata T, Asada A: Regulation of T cell apoptosis via T cell receptors and steroid receptors. Stem Cells 14: 632–641, 1996
15. Andreau K, Lemaire C, Souvannavong V, Adam A: Induction of apoptosis by dexamethasone in the B cell lineage. Immunopharmacology 40: 67–76, 1998
16. Xie H, Seward RJ, Huber BT: Cytokine rescue from glucocorticoid induced apoptosis in T cells is mediated through inhibition of Ikappa-Balpha. Mol Immunol 34: 987–994, 1997
17. Tan NS, Shaw NS, Vinckenbosch N, Liu P, Yasmin R, Desvergne B, Wahli W, Noy N: Selective cooperation between fatty acid binding proteins and peroxisome proliferator-activated receptors in regulating transcription. Mol Cell Biol 22: 5114–5127, 2002
18. Tautenhahn A, Brune B, von Knethen A: Activation-induced PPARgamma expression sensitizes primary human T cells toward apoptosis. J Leukoc Biol 73: 665–672, 2003
19. Padilla J, Leung E, Phipps RP: Human B lymphocytes and B lymphomas express PPAR-gamma and are killed by PPAR-gamma agonists. Clin Immunol 103: 22–33, 2002
20. Phillips M, Djian P, Green H: The nucleotide sequence of three genes participating in the adipose differentiation of 3T3 cells. J Biol Chem 261: 10821–10827, 1986
21. Guthmann F, Hohoff C, Fechner H, Humbert P, Borchers T, Spener F, Rustow B: Expression of fatty-acid-binding proteins in cells involved in lung-specific lipid metabolism. Eur J Biochem 253: 430–436, 1998
22. Kovacs B, Gulya K: Differential expression of multiple calmodulin genes in cells of the white matter of the rat spinal cord. Brain Res Mol Brain Res 102: 28–34, 2002
23. Amri EZ, Ailhaud G, Grimaldi P: Regulation of adipose cell differentiation. II. Kinetics of induction of the aP2 gene by fatty acids and modulation by dexamethasone. J Lipid Res 32: 1457–1463, 1991
24. Sun L, Nicholson AC, Hajjar DP, Gotto AM, Jr., Han J: Adipogenic differentiating agents regulate expression of fatty acid binding protein and CD36 in the J744 macrophage cell line. J Lipid Res 44: 1877–1886, 2003
25. Cook JS, Lucas JJ, Sibley E, Bolanowski MA, Christy RJ, Kelly TJ, Lane MD: Expression of the differentiation-induced gene for fatty acid-binding protein is activated by glucocorticoid and cAMP. Proc Natl Acad Sci USA 85: 2949–2953, 1988
26. Goleva E, Kisich KO, Leung DY: A role for STAT5 in the pathogenesis of IL-2-induced glucocorticoid resistance. J Immunol 169: 5934–5940, 2002
27. Semenkovich CF: Fatty acid metabolism and vascular disease. Trends Cardiovasc Med 14: 72–76, 2004
28. Rossi A, Kapahi P, Natoli G, Takahashi T, Chen Y, Karin M, Santoro MG: Anti-inflammatory cyclopentenone prostaglandins are direct inhibitors of IkappaB kinase. Nature 403: 103–108, 2000
29. Harris SG, Phipps RP: Peroxisome proliferator-activated receptor gamma (PPAR-gamma) activation in naive mouse T cells induces cell death. Ann N Y Acad Sci 905: 297–300, 2000
30. De Santis ML, Hammamieh R, Das R, Jett M: Adipocyte-fatty acid binding protein induces apoptosis in DU145 prostate cancer cells. J Exp Ther Oncol 4: 91–100, 2004
31. Zingarelli B, Sheehan M, Hake PW, O'Connor M, Denenberg A, Cook JA: Peroxisome proliferator activator receptor-gamma ligands, 15-deoxy-Delta(12,14)-prostaglandin J2 and ciglitazone, reduce systemic inflammation in polymicrobial sepsis by modulation of signal transduction pathways. J Immunol 171: 6827–6837, 2003

MOLECULAR AND CELLULAR BIOLOGY, July 2007, p. 5128–5134 Vol. 27, No. 14
0270-7306/07/$08.00+0 doi:10.1128/MCB.01072-06
Copyright © 2007, American Society for Microbiology. All Rights Reserved.

CD3 and Immunoglobulin G Fc Receptor Regulate Cerebellar Functions∇

Kazuhiro Nakamura,[1]* Hirokazu Hirai,[2] Takashi Torashima,[2] Taisuke Miyazaki,[3] Hiromichi Tsurui,[1] Yan Xiu,[1] Mareki Ohtsuji,[1] Qing Shun Lin,[1] Kazuyuki Tsukamoto,[1] Hiroyuki Nishimura,[4] Masao Ono,[5] Masahiko Watanabe,[3] and Sachiko Hirose[1]

Department of Pathology, Juntendo University School of Medicine, Tokyo 113-8421, Japan[1]; Department of Neurophysiology, Gunma University Graduate School of Medicine, Maebashi, Gunma 371-8511, Japan[2]; Department of Anatomy, Hokkaido University School of Medicine, Sapporo 060-8638, Japan[3]; Department of Biomedical Engineering, Toin University of Yokohama, Yokohama 225-8502, Japan[4]; and Department of Pathology, Tohoku University Graduate School of Medicine, Sendai 980-8575, Japan[5]

Received 15 June 2006/Returned for modification 16 July 2006/Accepted 23 April 2007

The immune and nervous systems display considerable overlap in their molecular repertoire. Molecules originally shown to be critical for immune responses also serve neuronal functions that include normal brain development, neuronal differentiation, synaptic plasticity, and behavior. We show here that FcγRIIB, a low-affinity immunoglobulin G Fc receptor, and CD3 are involved in cerebellar functions. Although membranous CD3 and FcγRIIB are crucial regulators on different cells in the immune system, both CD3ε and FcγRIIB are expressed on Purkinje cells in the cerebellum. Both CD3ε-deficient mice and FcγRIIB-deficient mice showed an impaired development of Purkinje neurons. In the adult, rotarod performance of these mutant mice was impaired at high speed. In the two knockout mice, enhanced paired-pulse facilitation of parallel fiber-Purkinje cell synapses was shared. These results indicate that diverse immune molecules play critical roles in the functional establishment in the cerebellum.

Some molecules originally shown to be critical for immune responses, such as the major histocompatibility complex (MHC) class I molecules, CD3ζ, and semaphorin 7A (3, 8, 15, 23), also serve neuronal functions. Based on studies of mutant mice, CD3ζ proved critical for the development of lateral geniculate nucleus (LGN) and long-term synaptic plasticity in the adult hippocampus (3, 8).

In the immune system, CD3 subunits are expressed on T cells. The T-cell receptor (TCR)–CD3 complex recognizing specific antigens bound to MHC present on antigen-presenting cells (APCs) is composed of a TCR heterodimer and CD3 polypeptides organized as dimers. The cell-cell interaction between APCs and T cells is known as an immunological synapse (5) in the mature immune system. In αβ T cells, when the TCR interacts with the antigen/MHC complex, it transmits information to a signal-transducing complex consisting of two CD3 subunit dimers, CD3ε-CD3γ and CD3ε-CD3δ, and the CD3ζ-CD3ζ homodimer (10). Among CD3 subunits, CD3ζ is a crucial subunit having three immunoreceptor tyrosine-based activation motifs (ITAMs), whereas the remaining subunits have one ITAM (25). Tyrosine residues within these motifs are phosphorylated by src family tyrosine kinases, and then Src homology 2-containing proteins, including the tyrosine kinase ZAP70, participate in signaling (13). The signaling in γδ TCRs is different from that in αβ TCRs. Most γδ TCRs lack CD3δ, and signal transduction by γδ TCR is superior to that by αβ TCR, as measured by its ability to induce calcium mobilization, extracellular signal-regulated kinase activation, and cellular proliferation (6).

FcγRIIB is a low-affinity membrane receptor for immune complexes broadly distributed on hematopoietic cells, such as B cells, mast cells, basophils, macrophages, eosinophils, neutrophils, dendritic cells, and Langerhans cells. FcγRIIB negatively regulates B-cell receptor-induced signaling in B cells via the inhibitory immunoreceptor tyrosine-based inhibition motif in its cytoplasmic domain (24, 30). Coengagement of the B-cell receptor and FcγRIIB results in the tyrosine phosphorylation of the immunoreceptor tyrosine-based inhibition motif and the recruitment of SHIP. SHIP, by hydrolyzing PIP3, causes the dissociation of Brutons tyrosine kinase from the membrane and the inhibition of calcium influx into the cell (29). Although the functional significance of FcγRIIB has been elucidated in hematopoietic cells, the physiological roles of FcγRIIB have not been explored in the nervous system.

The cerebellum is a key region operating motor learning and motor coordination. Cerebellar functions are regulated by coordinated neural networks. There are two major types of inputs to the cerebellum: climbing fibers (CFs) and mossy fibers. CFs are the axons of neurons located in the inferior olive. They enter the cerebellum and establish two branches, one to the deep nuclei and one to the Purkinje cells (PCs) of the cerebellar cortex. Mossy fibers synapse with the claw-like dendrites of the granule cells (GCs) in the cerebellar cortex. The GCs in turn communicate with the PC dendrites via their long parallel fiber (PF) axons. PC axons are the sole efferents from the cerebellar cortex.

Here, we found an unexpected common functional significance of CD3 and FcγRIIB in the cerebellum. Both CD3ε and

* Corresponding author. Mailing address: Department of Pathology, Juntendo University School of Medicine, Tokyo 113-8421, Japan. Phone: 81-3-5802-1039. Fax: 81-3-3813-3164. E-mail: kaz@med.juntendo.ac.jp.

∇ Published ahead of print on 14 May 2007.

Downloaded from mcb.asm.org at TOHOKU UNIVERSITY on March 27, 2008

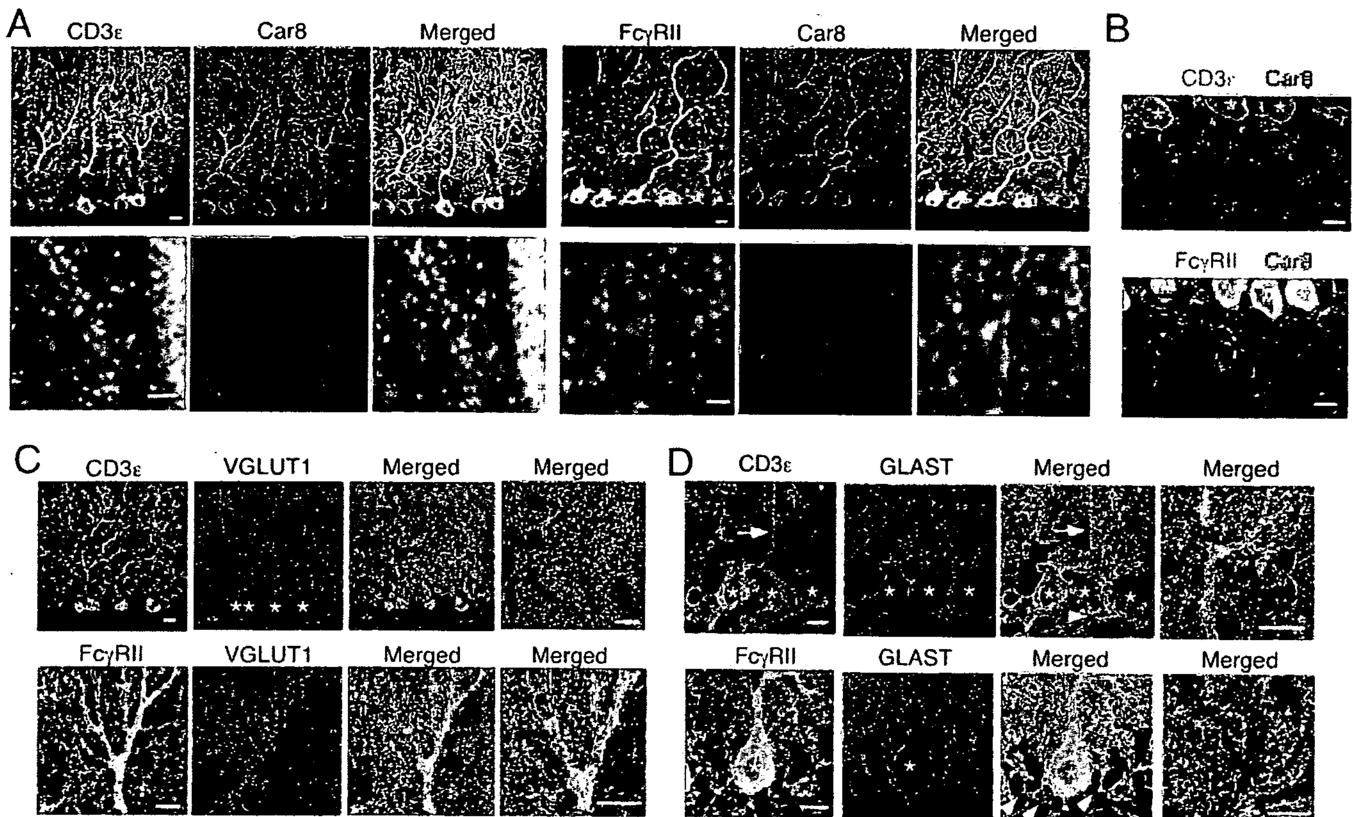

FIG. 1. Distribution of CD3ε and FcγRIIB in the cerebellum. Double immunofluorescence images are shown for CD3ε (green) or FcγRIIB (green) with Car8 (red) (A and B) in the molecular layer (A) and internal granular layer (B), with VGLUT1 (red) (C), or with GLAST (red) (D) in the cerebellum at P21. Arrows and arrowheads indicate rod-like staining of the Bergmann glia and the GLAST-positive cell bodies, respectively. Asterisks, Purkinje cell somata. Bars, 1 μm (A, lower panels) or 10 μm (A, upper panels, and B, C, and D).

FcγRIIB are located on Purkinje cells. CD3ε-deficient mice and FcγRIIB-deficient mice shared impaired development of Purkinje neurons, enhanced paired-pulse facilitation (PPF) of parallel fiber-Purkinje cell synapses, and poor rotarod performance at high speed.

MATERIALS AND METHODS

Animals. CD3ε knockout mice (16) with a C57BL/6 background were obtained from The European Mouse Mutant Archive. FcγRIIB knockout mice (30) with a C57BL/6 background were obtained from T. Takai (Tohoku Univ.). All animals were maintained according to the guidelines of Juntendo University.

RT-PCR. Reverse transcription-PCR (RT-PCR) was done using total RNA derived from the cerebellum and EL4 T-cell line and the following primers: *CD3ε* forward, 5′-AAGTCGAGGACAGTGGCTACTAC-3′, and reverse, 5′-CATCAGCAAGCCCAGAGTGATACA-3′; *CD3γ* forward, 5′-ATGGAGCAGAGGAAGGGTCTGGCT-3′, and reverse, 5′-CATTCTGTAATACACTTGCAGGGG-3′; *CD3δ* forward, 5′-GGAACAAATGTTGCTTGTCTGG-3′, and reverse, 5′-TCTTGGCAAACAGCAGTCGTA-3′; *CD3ζ* forward, 5′-AAGATGGCAGAAGCCTACAG-3′, and reverse, 5′-TTAATGACACAATGACCTTGC-3′; *CD3ζ* forward 5′-ACCCCAACCAGCTCTACAATGAG-3′, and reverse, 5′-AAGACGCTGGCACAGGATTGGCTA-3′. Primers for β-*actin* were purchased from Clontech (Palo Alto, CA).

Immunofluorescence staining. Immunofluorescence staining of the mouse cerebellum at postnatal day 21 (P21) was done essentially as described previously (20). The primary antibodies included anti-FcγRIIB (22), anti-CD3ε (145-2C11), anti-carbonic anhydrase 8 (Car8), anti-GLAST (26), anti-VGLUT1 (18), Alexa Fluor 488-labeled anticalbindin (Swant, Bellinzona, Switzerland), and Alexa Fluor 647-labeled anti-NeuN (Chemicon, Temecula, CA) antibodies. Anti-Car8 antibody was produced in the rabbit and guinea pig against 33 to 61 amino acid residues of the mouse Car8 (BC010773), and the specificity will be published elsewhere. Labeled sections were visualized with a confocal microscope (Zeiss LSM510). Quantitation of the pixel intensity of vGluT1 signals was carried out using Adobe PhotoShop and NIH Image.

Behavior. The performance on the rotarod (Ugo Basile, Comerio, Italy) was measured with a maximal observation time of 5 min. Animals were tested at a constant 5, 8, 10, or 30 rpm or an accelerating speed for two consecutive days, receiving four trials per day. The acceleration was started (2 rpm and the rod was rotating at ~30 rpm after 300 s), and the latency to fall was recorded.

Ambulation counts were made in an open field for 3 min essentially as described elsewhere (9). The behavioral tests were performed in a blind fashion.

Electrophysiology. Parasagittal cerebellar slices (200 μm) of the vermis were prepared from wild-type, FcγRIIB-deficient, and CD3ε-deficient mice (7). Slices were incubated at room temperature (25°C) for at least 1 h before recording. Whole-cell voltage clamp recordings were made of Purkinje cells visually identified at room temperature. The preparation was continuously superfused with an extracellular solution containing 124 mM NaCl, 2.5 mM KCl, 1.25 mM NaH_2PO_4, 1.5 mM $MgCl_2$, 2 mM $CaCl_2$, 26 mM $NaHCO_3$ and 20 mM glucose, which was bubbled continuously with a mixture of 95% O_2 and 5% CO_2. Patch pipettes had a resistance of 3 to 4 MΩ in the intracellular solution containing 135 mM Cs-D-gluconate, 15 mM CsCl, 1 mM $MgCl_2$, 10 mM HEPES, and 5 mM EGTA (pH 7.3). Picrotoxin (50 μM) was always present in the saline to block spontaneous inhibitory postsynaptic currents. To evoke PF or CF excitatory postsynaptic currents (EPSCs) from voltage-clamped Purkinje cells (−80 mV or 10 mV, respectively), square pulses (10 μs; 20 to 100 μA) were delivered every 10 s through a glass pipette with a tip 5 to 10 μm in diameter filled with 140 mM NaCl and 10 mM HEPES. To monitor the access resistance, a hyperpolarizing pulse (−10 mV; 50 ms) was applied 400 ms before the extracellular stimulation. Signals were filtered at 2 kHz and digitized at 4 kHz (Digidata 1320).

Statistics. Statistical significance was assessed using Student's *t* test unless otherwise noted. Analysis of variance was used for further analysis, and if there were significant differences, the Bonferroni test was used for post hoc analysis.

Downloaded from mcb.asm.org at TOHOKU UNIVERSITY on March 27, 2008